Johann Radon Institute for
Computational and Applied Mathematics
Austrian Academy of Sciences (ÖAW)

A FETI method for a TDNNS discretization of plane elasticity

A. Pechstein, C. Pechstein

RICAM-Report 2013-11

A FETI METHOD FOR A TDNNS DISCRETIZATION OF PLANE ELASTICITY*

ASTRID PECHSTEIN† AND CLEMENS PECHSTEIN‡

Abstract. In this article, we consider a hybridized tangential-displacement normal-normal-stress (TDNNS) discretization of linear elasticity. As shown in earlier work by Joachim Schöberl and the first author, TDNNS is a stable finite element discretization that does not suffers from volume locking. We propose a finite element tearing and interconnecting (FETI) method in order to solve the resulting linear system iteratively. The method is analyzed thoroughly for the compressible case in two dimensions, leading to a condition number bound of $C(1+\log(H/h))^2$, which coincides with known bounds of many other iterative substructuring methods. Numerical results confirm our theoretical findings. Furthermore, our experiments show that a certain instance of the method remains stable even in the almost incompressible limit.

Key words. linear elasticity, finite element method, TDNNS, iterative solvers, domain decomposition, FETI, almost incompressible

AMS subject classifications. 65N30, 65N22, 65N55, 74B05

1. Introduction.

The tangential-displacement normal-normal-stress (TDNNS) method is a mixed finite element method for linear elasticity, see [33]. Its main benefits are that the method is applicable both in case of nearly incompressible materials [38, Ch. 5] and for structurally anisotropic discretizations of slim domains by tensor product elements [34]. The TDNNS method is in between standard finite element discretizations using continuous elements for the displacement and mixed methods based on the dual Hellinger-Reissner formulation, where continuity of the normal stress vector is necessary. We refer to monographs such as [4, 21] for an introduction to standard continuous finite elements for elasticity, and [3, 1, 2] for mixed elements. While standard methods suffer from locking for both the nearly incompressible and the anisotropic case, the main drawback of conforming mixed methods is the large number of degrees of freedom per element. A recent contribution by Hauret and Hecht [20] presents a mixed method with continuous displacements and distributional stress fields, which satisfy an exact sequence property.

For a large number of mesh elements, the corresponding system of linear equations becomes too large to be solved directly (via matrix factorization), and so, one has to resort to iterative solvers. To the best of our knowledge, the present article is the first one addressing the efficient preconditioning of (a reformulation of) the TDNNS system of lowest polynomial order one. For the case of high polynomial order, an additive Schwarz block preconditioner has been proposed and analyzed in [38, Ch. 5], however, with one of the blocks being precisely the lowest order system.

Among the probably most efficient preconditioning techniques are multigrid and multilevel methods [19, 40], two-level overlapping Schwarz methods [39, Ch. 3], and a

*The second author gratefully acknowledges the former position at the Institute of Computational Mathematics, Johannes Kepler University Linz, Austria, where a substantial part of this research was carried out.

†Corresponding author, Institute of Technical Mechanics, Johannes Kepler University Linz, Altenberger Str. 69, 4040 Linz, Austria (phone: +43 732 2468 6299, fax: +43 732 2468 6282, e-mail: astrid.pechstein@jku.at)

‡Johann Radon Institute for Computational Mathematics (RICAM), Austrian Academy of Sciences, Altenberger Str. 69, 4040 Linz, Austria (phone: +43 732 2468 5257, fax: +43 732 2468 5212, e-mail: clemens.pechstein@oeaw.ac.at)

series of non-overlapping domain decomposition methods, also called iterative substructuring methods [39, Ch. 4–6]. The latter include the balancing Neumann-Neumann preconditioner [29], finite element tearing and interconnecting (FETI) methods [16, 17], with the variants dual-primal FETI (FETI-DP) [15], and total FETI (TFETI) [13, 32], and, finally, balancing domain decomposition by constraints (BDDC) [11], all of which have a number of components in common.

The main idea of FETI type methods is to decompose the computational domain into non-overlapping subdomains. On each subdomain, separate degrees of freedom are used, where the continuity of the displacement across subdomain interfaces is imposed by Lagrange multipliers. The resulting global system is of saddle-point structure. Careful elimination of the displacement leads to a *dual system* in the Lagrange multipliers, which is solved iteratively, usually by preconditioned conjugate gradients. In FETI and TFETI, a suitable projection is needed to allow for the elimination of the displacements in the floating subdomains which lack Dirichlet conditions. This projection acts as a coarse solve in the iterative method, such that the whole scheme has the flavor of a two-level method.

For conventional, continuous P^1-discretizations of the Poisson equation and of the primal formulation of linear elasticity, a rich analysis of FETI, TFETI, and FETI-DP is available, see, e.g., the articles [30, 26, 25] and the monographs [39, 35]. Under suitable regularity conditions on the mesh and subdomains, the condition number of the preconditioned dual system is bounded by $C(1 + \log(H/h))^2$, where H is the subdomain diameter, h the mesh parameter, and the constant C is independent of H, h, and as such of the number of subdomains. With the use of suitably chosen scalings in the method, C can even be made independent of certain jumps in the material parameters, see, e.g., [26, 39, 36, 35] (including jumps not resolved by the subdomain decomposition).

As mentioned above, the almost incompressible case already implies difficulties in the discretization itself, but even more in proper preconditioning. For related work on conventional discretizations with discontinuous pressure elements see, e.g., [24, 18, 12].

Recently, Victoriţa Dolean and coauthors have developed a symbolic approach to domain decomposition methods for systems of PDEs using the Smith factorization [10, 9]. The results (for a two half plane scenario) suggest that Neumann-Neumann and FETI preconditioners for linear elasticity should have certain robustness properties with respect to physical parameters, if the tangential displacement and the normal-normal stress traces are used for the inter-subdomain coupling. Whereas such a coupling can involve serious complications for conventional discretizations, it is most natural for the TDNNS method.

In the present article, we propose and analyze a FETI and TFETI method for a hybridized TDNNS discretization of linear elasticity in two dimensions. Under the assumptions that the subdomains and the mesh are sufficiently regular and that possible large jumps in the Young modulus are resolved by the subdomain decomposition, we are able to show the bound $C(1+\log(H/h))^2$ for the condition number, where the constant C is independent of H, h, and the jumps in Young's modulus. However, C depends on the subdomain shapes and on the Poisson ratio ν. The key tool of our analysis are two transformations between the TDNNS finite element space a space of standard continuous P^1 functions on a refined mesh, which allows to extend a series of classical tools for iterative substructuring methods to the TDNNS world.

The almost incompressible case is treated in experimental form: we show numerically that for a certain choice of parameters in the FETI method, the condition

number behaves quite robustly when Poisson's ratio ν tends to the incompressible limit 1/2. A rigorous analysis proving robustness with respect to ν is the subject of ongoing research.

The FETI method itself can be generalized in a straightforward way to the case of three dimensions. A generalization of our analysis, however, is not straightforward because of the presence of subdomain edges *and* faces, and also subject of future investigations.

The remainder of this paper is organized as follows. In Sect. 2, we fix some basic notation and describe the problem of linearized elasticity in two dimensions. Sect. 3 is devoted to the TDNNS formulation, in both mixed and hybridized form. Additionally, we discuss suitable discrete norms and the choice of degrees of freedom in the finite element method. In Sect. 4, we summarize the FETI algorithm with all its ingredients, such as the scaled Dirichlet preconditioner and suitable choices for a scaling matrix, $\underline{\mathbf{Q}}$. The analysis of the method (for the compressible case) is contained in Sect. 5. The paper ends with numerical results in Sect. 6. For the compressible case, we validate our theoretical findings. Moreover, we show experimentally that for a certain choice of ingredients the method behaves quite robustly towards the incompressible limit.

2. Preliminaries.

2.1. Notation. In the following, all vectors shall be denoted in boldface, while tensors or matrices are boldface and underlined. The i-th entry of a vector $\mathbf{u}$ shall be denoted by u_i, while B_{ij} is the (i,j) entry of a matrix $\underline{\mathbf{B}}$.

On the (Lipschitzian) boundary $\partial\Omega$ of a two-dimensional domain $\Omega \subset \mathbb{R}^2$, the outer unit normal vector shall be denoted by $\mathbf{n} = [n_1, n_2]^T$. The normal component v_n and tangential component $\mathbf{v}_t$ of a vector field $\mathbf{v}$ on the boundary are given by

$$v_n = \mathbf{v} \cdot \mathbf{n}, \qquad \mathbf{v}_t = \mathbf{v} - v_n \mathbf{n}. \tag{2.1}$$

For a tensor field $\underline{\boldsymbol{\sigma}}$, its (vector-valued) normal component $\boldsymbol{\sigma}_n$ can be split into a normal-normal component σ_{nn} and a normal-tangential component $\boldsymbol{\sigma}_{nt}$ by

$$\boldsymbol{\sigma}_n = \underline{\boldsymbol{\sigma}}\mathbf{n}, \qquad \sigma_{nn} = \boldsymbol{\sigma}_n \cdot \mathbf{n}, \qquad \boldsymbol{\sigma}_{nt} = \boldsymbol{\sigma}_n - \sigma_{nn}\mathbf{n}. \tag{2.2}$$

Concerning function spaces, we consistently use boldface symbols for vector-valued function spaces and boldface underlined symbols for tensor-valued function spaces. We use the Lebesgue space $L^2(\Omega)$ of square integrable functions on the domain Ω. $\underline{\mathbf{L}}^2_{sym}(\Omega)$ shall be the space of tensor-valued symmetric functions with components in $L^2(\Omega)$. Additionally, we need the space $L^2(e)$ defined on a one-dimensional manifold e. $H^1(\Omega)$ shall denote the usual Sobolev space of L^2 functions with weak gradient in $\mathbf{L}^2(\Omega)$. We define the standard curl operator curl mapping vector-valued functions to scalars, the divergence operator div and the row-wise divergence **div** mapping tensors to vectors,

$$\operatorname{curl}(\mathbf{v}) = \frac{\partial v_2}{\partial x_1} - \frac{\partial v_1}{\partial x_2}, \quad \operatorname{div}(\mathbf{v}) = \frac{\partial v_1}{\partial x_1} + \frac{\partial v_2}{\partial x_2}, \quad \mathbf{div}(\underline{\boldsymbol{\sigma}}) = \begin{bmatrix} \frac{\partial \sigma_{11}}{\partial x_1} + \frac{\partial \sigma_{12}}{\partial x_2} \\ \frac{\partial \sigma_{21}}{\partial x_1} + \frac{\partial \sigma_{22}}{\partial x_2} \end{bmatrix}. \tag{2.3}$$

$\mathbf{H}(\operatorname{curl}, \Omega)$ and $\mathbf{H}(\operatorname{div}, \Omega)$ are the usual spaces of vector-valued L^2 functions with weak curl or divergence in $L^2(\Omega)$, respectively. If clear from the context, the indication of the domain is omitted. By P^k we denote the space of polynomials up to order k.

The dual space of a Hilbert space V shall be denoted by an asterisk V^*. The duality pairing is indicated by angles $\langle \cdot, \cdot \rangle_{V^* \times V}$. If clear from the context, the space subscript can be omitted.

2.2. Linear Elasticity in Two Dimensions. Let $\Omega \subset \mathbb{R}^2$ be a bounded, connected domain with Lipschitz boundary $\partial\Omega$. We are interested in finding the displacement vector $\mathbf{u} = [u_1, u_2]^T$ and the stress tensor $\underline{\boldsymbol{\sigma}}$ subject to the assumptions of linear elasticity, volume forces $\mathbf{f}_V$, and boundary conditions. The boundary $\partial\Omega$ shall be divided into the disjoint parts Γ_D and Γ_N, with $\partial\Omega = \overline{\Gamma_D} \cup \overline{\Gamma_N}$ and $|\Gamma_D| > 0$. On the first part Γ_D, displacement boundary conditions are prescribed, while on Γ_N surface traction are applied. The complete set of equations reads: find $\mathbf{u} : \Omega \to \mathbb{R}^2$ such that

$$\mathbf{div}\underline{\boldsymbol{\sigma}} = -\mathbf{f}_V \qquad \text{in } \Omega, \tag{2.4}$$

$$\underline{\boldsymbol{\sigma}} = \underline{\mathbf{D}}\,\underline{\boldsymbol{\varepsilon}}(\mathbf{u}) \qquad \text{in } \Omega, \text{ where } \underline{\boldsymbol{\varepsilon}}(\mathbf{u}) = \tfrac{1}{2}\left(\nabla\mathbf{u} + (\nabla\mathbf{u})^T\right), \tag{2.5}$$

$$\mathbf{u} = \mathbf{u}_D \qquad \text{on } \Gamma_D, \tag{2.6}$$

$$\boldsymbol{\sigma}_n = \mathbf{t}_N \qquad \text{on } \Gamma_N, \tag{2.7}$$

where $\mathbf{u}_D$, $\mathbf{f}_V$, and $\mathbf{t}_N$ are given, and the 4^{th} order tensor $\underline{\mathbf{D}}$ implements Hooke's linear material law in the known way, based on Young's modulus E and Poisson's ratio ν.

2.3. Triangulation. For the discretization of the above equations in a finite element scheme, we need a triangulation of the computational domain Ω. We assume that the domain Ω is polygonal, and that $\mathcal{T}_h(\Omega) = \bigcup\{T\}$ forms a shape-regular simplicial triangulation of Ω. For simplicity of presentation, we assume that the triangulation is quasi-uniform with mesh size $h \simeq \operatorname{diam}(T)$ for all elements T. The theory below, however, can easily be generalized to shape-regular meshes using local mesh sizes $h_T = \operatorname{diam}(T)$.

Throughout the paper, an expression of the form $a \lesssim b$ stands for $a \leq C\,b$ where C is a constant independent of h, in particular just depending on the shape-regularity and quasi-uniformity constants of the triangulation as well as the shape of the underlying domain. In all cases below, this domain is *local*, i.e., a subdomain. Moreover, $a \simeq b$ is a short-hand for $a \lesssim b$ and $b \lesssim a$.

3. TDNNS Formulation. In the current section, the tangential displacement normal-normal stress (TDNNS) formulation as introduced in [33] shall be presented shortly. Hybridization of the method is discussed, as it is needed for the FETI analysis and implementation. For simplicity of presentation, we restrict ourselves to the case of homogeneous displacement and traction boundary conditions, setting $\mathbf{u}_D = 0$ and $\mathbf{t}_N = 0$. The extension to the inhomogeneous case is straightforward but would require much more notation.

3.1. Mixed Formulation. Most standard methods for the elasticity problem rely on a primal formulation, which is obtained eliminating the stress tensor $\underline{\boldsymbol{\sigma}}$ from equation (2.4). Then one searches for the displacement $\mathbf{u} \in \mathbf{H}^1(\Omega)$ with $\mathbf{u}|_{\Gamma_D} = 0$ such that

$$\int_\Omega \underline{\mathbf{D}}\,\underline{\boldsymbol{\varepsilon}}(\mathbf{u}) : \underline{\boldsymbol{\varepsilon}}(\mathbf{v})\,dx = \int_\Omega \mathbf{f}_V \cdot \mathbf{v}\,dx \qquad \forall \mathbf{v} \in \mathbf{H}^1(\Omega),\ \mathbf{v}|_{\Gamma_D} = 0. \tag{3.1}$$

In a conforming finite element method, the displacement vector $\mathbf{u}$ is approximated by a continuous finite element function.

The TDNNS method is a mixed method, where displacement and stresses are approximated by separate unknowns. In [33] we have derived a method, where the displacement $\mathbf{u}$ is sought in the vector-valued space $\mathbf{H}(\text{curl})$, while the stresses lie

in the newly introduced tensor-valued space $\underline{\mathbf{H}}(\mathrm{div}\mathbf{div})$. In the current work, we use the lowest-order TDNNS finite element spaces from [33]: for the displacements, tangential continuous elements from the second family of Nédélec [31], and for the stresses a newly introduced space of tensor-valued normal-normal continuous finite elements,

$$\mathbf{V}_h := \{\mathbf{v} \in \mathbf{L}^2 : \mathbf{v}|_T \in \mathbf{P}^1 \ \forall T \in \mathcal{T}_h, \mathbf{v}_t \text{ continuous}, \mathbf{v}_t = 0 \text{ on } \Gamma_D\}, \tag{3.2}$$

$$\underline{\boldsymbol{\Sigma}}_h := \{\underline{\boldsymbol{\sigma}} \in \underline{\mathbf{L}}^2_{sym} : \underline{\boldsymbol{\sigma}}|_T \in \underline{\mathbf{P}}^1 \ \forall T \in \mathcal{T}_h, \sigma_{nn} \text{ continuous}, \sigma_{nn} = 0 \text{ on } \Gamma_N\}. \tag{3.3}$$

The mixed system based on the two equations (2.4)–(2.5) reads: find $\mathbf{u} \in \mathbf{V}_h$ and $\underline{\boldsymbol{\sigma}} \in \underline{\boldsymbol{\Sigma}}_h$ such that

$$\int_\Omega \underline{\mathbf{D}}^{-1}\underline{\boldsymbol{\sigma}} : \underline{\boldsymbol{\tau}}\, dx + \langle \mathbf{div}\underline{\boldsymbol{\tau}}, \mathbf{u}\rangle = 0 \qquad \forall \underline{\boldsymbol{\tau}} \in \underline{\boldsymbol{\Sigma}}_h, \tag{3.4}$$

$$\langle \mathbf{div}\underline{\boldsymbol{\sigma}}, \mathbf{v}\rangle = -\int_\Omega \mathbf{f}_V \cdot \mathbf{v}\, dx \qquad \forall \mathbf{v} \in \mathbf{V}_h. \tag{3.5}$$

The duality product $\langle \mathbf{div}\underline{\boldsymbol{\sigma}}, \mathbf{u}\rangle$ is well defined in the infinite-dimensional Hilbert space setting (see [33]). For finite element functions $\underline{\boldsymbol{\sigma}} \in \underline{\boldsymbol{\Sigma}}_h$ and $\mathbf{u} \in \mathbf{V}_h$, the duality product $\langle \mathbf{div}\underline{\boldsymbol{\sigma}}, \mathbf{u}\rangle$ can be evaluated by element-wise volume and boundary integrals:

$$\langle \mathbf{div}\underline{\boldsymbol{\sigma}}, \mathbf{u}\rangle = \sum_{T\in\mathcal{T}_h} \left(\int_T \mathbf{div}\underline{\boldsymbol{\sigma}} \cdot \mathbf{u}\, dx - \int_{\partial T} \boldsymbol{\sigma}_{nt}\mathbf{u}_t\, ds \right). \tag{3.6}$$

In [33] we have shown that the method described above leads to a stable saddle-point system, which can be analyzed using Brezzi's theory [8, Theorem 1.1].

3.2. Hybridization. For the FETI analysis and implementation we use an equivalent variant of the original TDNNS method obtained by hybridization of the stresses. Then, the stress finite elements are totally discontinuous, and all coupling degrees of freedom are connected to displacement quantities. While the original system matrix is indefinite, it becomes symmetric positive definite in the hybridized case. For details on the method, its analysis and application to the nearly incompressible case, see [38, Ch. 5].

So far, we used conforming finite element spaces $\underline{\boldsymbol{\Sigma}}_h$ and $\mathbf{V}_h$ satisfying normal-normal and tangential continuity, respectively. Hybridization means that the normal-normal continuity of the flux space $\underline{\boldsymbol{\Sigma}}_h$ is broken, and that the continuity is enforced by Lagrangian multipliers. We define the discontinuous stress space

$$\widetilde{\underline{\boldsymbol{\Sigma}}}_h := \{\underline{\boldsymbol{\sigma}} \in \underline{\mathbf{L}}^2_{sym} : \underline{\boldsymbol{\sigma}}|_T \in \underline{\mathbf{P}}^1 \ \forall T \in \mathcal{T}_h\}. \tag{3.7}$$

The Lagrangian multipliers will correspond to normal displacements on element interfaces, and shall be denoted by $\overline{u}_n$. They will be discretized by edge-wise P^1 functions. Note that, for two adjacent elements T_1 and T_2, the normal component u_n of a continuous displacement field $\mathbf{u}$ changes its sign when switching from T_1 to T_2 due to the opposing outer normals, $u_{n_{T_1}} = -u_{n_{T_2}}$. Accordingly, it is convenient formally construct a Lagrange multiplier space with the same property. To this end, let $\partial\mathcal{T}_h = \bigcup_{T\in\mathcal{T}_h}\{\partial T\}$ denote the union of all element boundaries, not identifying coincident boundary parts. Then a function in $L^2(\partial\mathcal{T}_h)$ has two independent values on an element interface when considering it as a part of the two respective element boundaries. A Lagrangian multiplier $\overline{v}_n$ satisfies the "continuity assumption" that

its sign changes when switching from one boundary part to the other on an element interface. Therefore, we define

$$\begin{aligned}\overline{V}_{n,h} \;:=\; \big\{&\overline{v}_n \in L^2(\partial\mathcal{T}_h) : \forall \text{ edge } e \subset \partial T : \overline{v}_n|_e \in P^1,\\ &\overline{v}_n|_{\partial T_1} = -\overline{v}_n|_{\partial T_2} \text{ on } \partial T_1 \cap \partial T_2,\ \overline{v}_n|_{\partial\Gamma_D} = 0\big\}.\end{aligned} \tag{3.8}$$

In an implementation a typical Lagrangian multiplier from $\overline{V}_{n,h}$ can be defined as a piecewise polynomial function on element edges, choosing unique edge normal directions. Note that the edge-wise polynomial order of the Lagrange multiplier space coincides with that of the broken normal-normal stress, thus also the number of Lagrangian multipliers coincides with the number of broken normal-normal continuity constraints. The normal-normal continuity condition for $\underline{\boldsymbol{\sigma}} \in \widetilde{\underline{\boldsymbol{\Sigma}}}_h$, together with the traction condition $\sigma_{nn}|_{\Gamma_N} = 0$, is equivalent to

$$\sum_{T\in\mathcal{T}_h} \int_{\partial T} \sigma_{nn}\overline{v}_n \, ds \;=\; 0 \qquad \forall\, \overline{v}_n \in \overline{V}_{n,h}. \tag{3.9}$$

The finite element equations (3.4)–(3.5) can be rewritten equivalently in hybridized form: find $\underline{\boldsymbol{\sigma}} \in \widetilde{\underline{\boldsymbol{\Sigma}}}_h$, $\mathbf{u} \in \mathbf{V}_h$ and $\overline{u}_n \in \overline{V}_{n,h}$ such that

$$\mathcal{A}(\underline{\boldsymbol{\sigma}}, (\mathbf{u}, \overline{u}_n); \underline{\boldsymbol{\tau}}, (\mathbf{v}, \overline{v}_n)) = \mathcal{F}(\mathbf{v}, \overline{v}_n) \qquad \forall\, \underline{\boldsymbol{\tau}} \in \widetilde{\underline{\boldsymbol{\Sigma}}}_h,\, \mathbf{v} \in \mathbf{V}_h,\, \overline{v}_n \in \overline{V}_{n,h}, \tag{3.10}$$

with bilinear form $\mathcal{A}$ and linear form $\mathcal{F}$, given by

$$\begin{aligned}\mathcal{A}(\underline{\boldsymbol{\sigma}}, (\mathbf{u}, \overline{u}_n); \underline{\boldsymbol{\tau}}, (\mathbf{v}, \overline{v}_n)) \;:=\; &\int_\Omega \underline{\mathbf{D}}^{-1}\underline{\boldsymbol{\sigma}} : \underline{\boldsymbol{\tau}}\, dx + \langle \mathbf{div}\underline{\boldsymbol{\tau}}, \mathbf{u}\rangle + \langle \mathbf{div}\underline{\boldsymbol{\sigma}}, \mathbf{v}\rangle\\ &- \sum_{T\in\mathcal{T}_h} \int_{\partial T} \big(\tau_{nn}\overline{u}_n + \sigma_{nn}\overline{v}_n\big)\, ds,\end{aligned} \tag{3.11}$$

$$\mathcal{F}(\mathbf{v}, \overline{v}_n) \;:=\; -\int_\Omega \mathbf{f}_V \cdot \mathbf{v}\, dx. \tag{3.12}$$

Note that the bilinear form $\mathcal{A}$ can be evaluated element-wise as in (3.6). To treat non-homogeneous traction boundary conditions, the right hand side $\mathcal{F}$ has to be augmented by the surface integral $-\int_{\Gamma_N} \mathbf{t}_{N,t} \cdot \mathbf{v}_t + t_{N,n}\overline{v}_n \, ds$.

3.3. Stability and Discrete Norms. In [33, 38], a stability analysis for the (hybridized) TDNNS method based on Brezzi's Theory (cf. [8, Theorem 1.1]) was carried out. In particular, the mixed system (3.10) is stable with respect to the following (semi-)norms,

$$|\mathbf{v}, \overline{v}_n|^2_{\mathbf{H}(\underline{\boldsymbol{\varepsilon}},\Omega,\mathcal{T}_h)} \;:=\; \sum_{T\in\mathcal{T}_h} \Big(\|\underline{\boldsymbol{\varepsilon}}(\mathbf{v})\|^2_{\underline{\mathbf{L}}^2(T)} + h^{-1}\|v_n - \overline{v}_n\|^2_{L^2(\partial T)}\Big), \tag{3.13}$$

$$\|\underline{\boldsymbol{\sigma}}\|_{\underline{\boldsymbol{\Sigma}}_h} \;:=\; \|\underline{\boldsymbol{\sigma}}\|_{\underline{\mathbf{L}}^2(\Omega)}. \tag{3.14}$$

Note that $|\mathbf{v}, \overline{v}_n|_{\mathbf{H}(\underline{\boldsymbol{\varepsilon}},\Omega,\mathcal{T}_h)}$ is a norm for non-trivial displacement boundary conditions. Assuming H^2-regularity for the displacement and H^1 regularity for the stresses, the error measured in the above pair of norms is $\mathcal{O}(h)$.

The above norms will also be used in our analysis, with Ω being replaced by a subdomain. We also need other norms, where in the following, Ω can be seen as a *generic* subdomain. The semi-norm of broken H^1 type

$$|\mathbf{v}, \overline{v}_n|^2_{\mathbf{H}^1(\Omega,\mathcal{T}_h)} \;:=\; \sum_{T\in\mathcal{T}_h} \Big(|\mathbf{v}|^2_{\mathbf{H}^1(T)} + h^{-1}\|v_n - \overline{v}_n\|^2_{L^2(\partial T)}\Big) \tag{3.15}$$

forms an equivalent norm to (3.13) in case the (infinitesimal) rigid body motions are fixed, e.g., by displacement boundary conditions [7]. By adding an L^2 term, the semi-norms can be augmented to equivalent full norms also in cases where rigid body motions are present in the finite element spaces. We use a proper scaling of the L^2 term leading to a (squared) norm equivalent to the semi-norm (3.15) in case of fixed rigid body motions,

$$\|\mathbf{v}, \overline{v}_n\|^2_{\mathbf{H}^1(\Omega,\mathcal{T}_h)} := |\mathbf{v}, \overline{v}_n|^2_{\mathbf{H}^1(\Omega,\mathcal{T}_h)} + \frac{1}{\operatorname{diam}(\Omega)^2}\|\mathbf{v}\|^2_{\mathbf{L}^2(\Omega)}. \tag{3.16}$$

In all norms, the global mesh size h above can be replaced by the local mesh size $h_T := \operatorname{diam}(T)$, leading to refined results for non-uniform triangulations.

With the next lemma, we observe that $\|\mathbf{v}, \overline{v}_n\|_{\mathbf{H}^1(\Omega,\mathcal{T}_h)}$ bounds a properly scaled L^2-norm of the normal displacement $\overline{v}_n$.

LEMMA 3.1. *For* $(\mathbf{v}, \overline{v}_n) \in \mathbf{V}_h \times \overline{V}_{n,h}$,

$$\frac{1}{\operatorname{diam}(\Omega)^2} \sum_{T\in\mathcal{T}_h} h \, \|\overline{v}_n\|^2_{L^2(\partial T)} \lesssim \|\mathbf{v}, \overline{v}_n\|^2_{\mathbf{H}^1(\Omega,\mathcal{T}_h)}. \tag{3.17}$$

Proof. Let the element T and the edge $e_{jk} \subset \partial T$ be fixed. By the triangle inequality, $|v_n| \le |\mathbf{v}|$, and transformation to the reference element, we obtain

$$\begin{aligned} h \, \|\overline{v}_n\|^2_{L^2(e_{jk})} &\lesssim h \, \|v_n - \overline{v}_n\|^2_{L^2(e_{jk})} + h \, \|v_n\|^2_{L^2(e_{jk})} \\ &\lesssim h \, \|v_n - \overline{v}_n\|^2_{L^2(e_{jk})} + \|\mathbf{v}\|^2_{\mathbf{L}^2(T)}. \end{aligned} \tag{3.18}$$

Estimate (3.17) is obtained from (3.18) by summing over all edges and elements and using that $h/\operatorname{diam}(\Omega)^2 \le h^{-1}$. ∎

3.4. Degrees of Freedom. For the space $\mathbf{V}_h$, defined in (3.2), we use the second family of Nédélec elements with the following degrees of freedom (dofs) associated to each edge e:

$$\mathbf{v} \mapsto \int_e \mathbf{v}_t \, ds, \qquad \mathbf{v} \mapsto \frac{1}{|e|}\int_e \mathbf{v}_t \, s \, ds, \tag{3.19}$$

where $\mathbf{v}_t$ is the corresponding tangential component according to (2.1), and $|e|$ the length of edge e. For the space $\overline{V}_{n,h}$, that is defined edge-wise, we use scaled nodal dofs:

$$\overline{v}_n|_e \mapsto |e| \, \overline{v}_n|_e(N_1), \qquad \overline{v}_n|_e \mapsto |e| \, \overline{v}_n|_e(N_2),$$

where N_1 and N_2 are the endpoints of edge e. We stress that these dofs are *associated to edges* rather than vertices, because of the discontinuous nature of $\overline{V}_{n,h}$. For a sketch of the dofs of an element see Figure 3.1.

Any pair of displacement functions $(\mathbf{u}, \overline{u}_n) \in \mathbf{V}_h \times \overline{V}_{n,h}$ can be identified with a vector $\mathbf{U}$ holding its dofs. This identification between a pair of functions and a system vector shall be denoted by

$$(\mathbf{u}, \overline{u}_n) \leftrightarrow \mathbf{U}. \tag{3.20}$$

Collecting the dofs of the stress tensor $\underline{\boldsymbol{\sigma}} \in \widetilde{\underline{\boldsymbol{\Sigma}}}_h$ in a system vector $\mathbf{S}$, the bilinear form $\mathcal{A}$ corresponds uniquely to a system matrix $\underline{\mathbf{A}}$ of the standard saddle point form

$$\underline{\mathbf{A}} = \begin{bmatrix} \mathbf{A_{SS}} & \mathbf{A_{SU}} \\ \mathbf{A_{SU}}^T & 0 \end{bmatrix}. \tag{3.21}$$

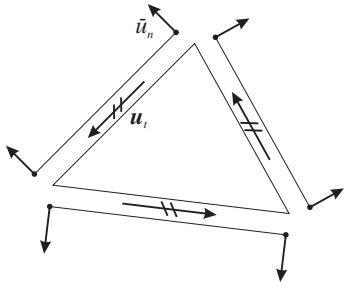

FIG. 3.1. *Triangular finite element and its coupling degrees of freedom associated to the displacement* $(\mathbf{u}, \overline{u}_n)$ *for the hybridized TDNNS method.*

As the dofs of the stress space $\widetilde{\underline{\boldsymbol{\Sigma}}}_h$ are totally local to each element, the upper left part $\underline{\mathbf{A}}_{\mathbf{SS}}$ is block diagonal and can be inverted easily. This procedure, called static condensation, leads to the symmetric positive definite system

$$\underline{\mathbf{K}}\mathbf{U} = \mathbf{F}, \tag{3.22}$$

with (negative) Schur complement $\underline{\mathbf{K}} = \underline{\mathbf{A}}_{\mathbf{SU}}^T \underline{\mathbf{A}}_{\mathbf{SS}}^{-1} \underline{\mathbf{A}}_{\mathbf{SU}}$ and load vector $\mathbf{F}$ corresponding to $\mathcal{F}$. The bilinear form corresponding to $\underline{\mathbf{K}}$ is coercive and bounded with respect to the (semi-)norm $|\mathbf{v}, \overline{v}_n|_{\mathbf{H}(\underline{\boldsymbol{\varepsilon}}, \Omega, \mathcal{T}_h)}$, cf. [33].

In the following, we shall consider two variants of incorporating the (homogeneous) displacement boundary conditions.

(a) The dofs associated to edges on $\overline{\Gamma}_D$ are not present in the system.
(b) All dofs associated to $\overline{\Gamma}_D$ *are* present in the system, but subject to explicit constraints (to be described later on).

In variant (b), we call the dofs associated to Γ_D *Dirichlet dofs*.

4. The FETI Algorithm. In this section, we describe the FETI algorithm for the hybridized TDNNS method. This algorithm is an iterative solver for (a reformulation of) equation (3.22).

4.1. Tearing and Interconnecting. We consider a non-overlapping partition of Ω into subdomains $\Omega^{(i)}$:

$$\overline{\Omega} \;=\; \bigcup_{i=1}^{N} \overline{\Omega}^{(i)},$$

such that each subdomain is the union of elements of the global mesh $\mathcal{T}_h(\Omega)$. An upper index (i) shall indicate an association to subdomain $\Omega^{(i)}$; $\mathcal{T}_h^{(i)}$ denotes the subdomain mesh resulting from the restriction of $\mathcal{T}_h$ to $\Omega^{(i)}$. Additionally, $\mathbf{V}_h^{(i)}$ and $\overline{V}_{n,h}^{(i)}$ are the restriction of the respective global finite element spaces to $\mathcal{T}_h^{(i)}$.

Let $\underline{\mathbf{K}}^{(i)}$ denote the subdomain stiffness matrix assembled over the elements T of $\mathcal{T}_h^{(i)}$, and let $\mathbf{F}^{(i)}$ denote the corresponding subdomain load vector.

The dofs on $\overline{\Omega}^{(i)} \setminus \overline{\Gamma}_D$ can be subdivided into two groups:

- *Coupling dofs*, that are shared with one of the other subdomains, i.e., being associated to an edge on the *interface* $\Gamma := \bigcup_{i \neq j = 1}^{N} (\partial\Omega_i \cap \partial\Omega_j)$.
- *Interior dofs*, which are not coupling.

In our 2D setting, coupling dofs are always shared by two subdomains. We write

$$(i,k) \;\sim\; (j,\ell),$$

if a coupling dof k on $\partial\Omega_i$ corresponds to dof ℓ on $\partial\Omega_j$. Recall that in variant (b) above, there is the third group of *Dirichlet dofs*. We write

$$(i,k) \;\sim\; \Gamma_D$$

to express the fact that dof k on $\partial\Omega_i$ is a Dirichlet dof.

Let $n^{(i)}$ denote the total number of dofs on $\overline{\Omega}^{(i)}$ (including possible Dirichlet dofs). Let $\mathbf{U}^{(i)} \in \mathbb{R}^{n^{(i)}}$ be vectors containing the displacement dofs of the finite element systems and let $\underline{\mathbf{B}}^{(i)} \in \mathbb{R}^{M\times n^{(i)}}$, $i = 1,\ldots,N$ be signed Boolean matrices such that each row of

$$\sum_{i=1}^{N} \underline{\mathbf{B}}^{(i)}\mathbf{U}^{(i)} \;=\; 0$$

corresponds to a constraint of the form

$$U_k^{(i)} - U_\ell^{(j)} \;=\; 0 \qquad \text{for } (i,k)\sim(j,\ell)$$

or – in variant (b) – a constraint of the form

$$U_k^{(i)} \;=\; 0 \qquad \text{for } (i,k)\sim\Gamma_D\,.$$

Above, M denotes the total number of such constraints.

With these notations, the global finite element system can be reformulated as the saddle point problem

$$\begin{bmatrix} \underline{\mathbf{K}} & \underline{\mathbf{B}}^\top \\ \underline{\mathbf{B}} & 0 \end{bmatrix} \begin{bmatrix} \mathbf{U} \\ \boldsymbol{\lambda} \end{bmatrix} \;=\; \begin{bmatrix} \mathbf{F} \\ 0 \end{bmatrix} \tag{4.1}$$

with the block matrices $\underline{\mathbf{K}} := \operatorname{diag}(\underline{\mathbf{K}}^{(i)})_{i=1}^N$, $\underline{\mathbf{B}} := [\underline{\mathbf{B}}^{(1)}|\ldots|\underline{\mathbf{B}}^{(N)}]$ and the block vectors $\mathbf{U} := [(\mathbf{U}^{(1)})^\top|\ldots|(\mathbf{U}^{(N)})^\top]^\top$, $\mathbf{F} := [(\mathbf{F}^{(1)})^\top|\ldots|(\mathbf{F}^{(N)})^\top]^\top$. In our 2D setting, there are no redundant constraints: $\ker(\underline{\mathbf{B}}^\top) = \{0\}$. From the Dirichlet conditions and the properties of the global stiffness matrix, one can conclude that $\ker(\underline{\mathbf{K}}) \cap \ker(\underline{\mathbf{B}}) = \{0\}$, which implies that (4.1) has a unique solution. Using variant (a) we speak of a FETI method, whereas in variant (b) of a total FETI (TFETI) method, cf. [13, 32].

4.2. Elimination of Displacements. As for the classical FETI method [16, 17] and the TFETI variant [13], we fix full-rank matrices $\underline{\mathbf{R}}^{(i)}$ such that

$$\operatorname{range}(\underline{\mathbf{R}}^{(i)}) \;=\; \ker(\underline{\mathbf{K}}^{(i)}) \tag{4.2}$$

and set $\underline{\mathbf{R}} := \operatorname{diag}(\underline{\mathbf{R}}_i)_{i=1}^N$. In variant (b), $\dim(\ker(\underline{\mathbf{K}}^{(i)})) = 3$ for all subdomains $\Omega^{(i)}$. E.g., the columns of $\underline{\mathbf{R}}_i$ are obtained by evaluating the dofs from Sect. 3.4 at the (infinitesimal) rigid body motions and their normal components.

Let $(\underline{\mathbf{K}}^{(i)})^\dagger \in \mathbb{R}^{n^{(i)}\times n^{(i)}}$ denote a generalized inverse of $\underline{\mathbf{K}}^{(i)}$, with the only requirement that

$$\underline{\mathbf{K}}^{(i)}(\underline{\mathbf{K}}^{(i)})^\dagger\mathbf{G} \;=\; \mathbf{G} \qquad \forall \mathbf{G} \in \operatorname{range}(\underline{\mathbf{K}}^{(i)}),$$

Algorithm 1: FETI method to solve (4.1).

$\boldsymbol{\lambda}_0 := \underline{\mathbf{Q}}\underline{\mathbf{G}}(\underline{\mathbf{G}}^\top\underline{\mathbf{Q}}\underline{\mathbf{G}})^{-1}\underline{\mathbf{R}}^\top\mathbf{F}$
Find $\widetilde{\boldsymbol{\lambda}} \in \boldsymbol{\Lambda}_{\mathrm{ad}}$: $\quad \underline{\mathbf{P}}^\top\underline{\mathbf{F}}\widetilde{\boldsymbol{\lambda}} \;=\; \underline{\mathbf{P}}^\top\underline{\mathbf{B}}\,\underline{\mathbf{K}}^\dagger(\mathbf{F} - \underline{\mathbf{B}}^\top\boldsymbol{\lambda}_0)$
$\boldsymbol{\lambda} := \boldsymbol{\lambda}_0 + \widetilde{\boldsymbol{\lambda}}$
$\boldsymbol{\xi} := -(\underline{\mathbf{G}}^\top\underline{\mathbf{Q}}\underline{\mathbf{G}})^{-1}\underline{\mathbf{G}}^\top\underline{\mathbf{Q}}\underline{\mathbf{B}}\,\underline{\mathbf{K}}^\dagger(\mathbf{F} - \underline{\mathbf{B}}^\top\boldsymbol{\lambda})$
$\mathbf{U} := \underline{\mathbf{K}}^\dagger(\mathbf{F} - \underline{\mathbf{B}}^\top\boldsymbol{\lambda}) + \underline{\mathbf{R}}\boldsymbol{\xi}$

and set $\underline{\mathbf{K}}^\dagger := \mathrm{diag}((\underline{\mathbf{K}}^{(i)})^\dagger)_{i=1}^N$. Several possibilities of realizing $(\underline{\mathbf{K}}^{(i)})^\dagger$ have been proposed in the literature, see, e.g. [16, Appendix I], [14], as well as [28] and the references therein. A further option is sketched in Sect. 6.

Elimination of the primal unknowns $\mathbf{U}$ in (4.1) leads to the saddle point problem

$$\begin{bmatrix} \underline{\mathbf{F}} & -\underline{\mathbf{G}} \\ \underline{\mathbf{G}}^\top & 0 \end{bmatrix} \begin{bmatrix} \boldsymbol{\lambda} \\ \boldsymbol{\xi} \end{bmatrix} \;=\; \begin{bmatrix} \underline{\mathbf{B}}\,\underline{\mathbf{K}}^\dagger\mathbf{F} \\ \underline{\mathbf{R}}^\top\mathbf{F} \end{bmatrix}, \tag{4.3}$$

where

$$\underline{\mathbf{F}} \;:=\; \underline{\mathbf{B}}\,\underline{\mathbf{K}}^\dagger\underline{\mathbf{B}}^\top, \qquad \underline{\mathbf{G}} \;:=\; \underline{\mathbf{B}}\,\underline{\mathbf{R}}\,. \tag{4.4}$$

4.3. Projection Method. System (4.3) is solved by a projection method. Let $\underline{\mathbf{Q}} \in \mathbb{R}^{M\times M}$ be a symmetric positive semi-definite matrix (yet to be specified) such that $\underline{\mathbf{Q}}$ is definite on range($\underline{\mathbf{G}}$), and define the projection

$$\underline{\mathbf{P}} \;:=\; \underline{\mathbf{I}} - \underline{\mathbf{Q}}\underline{\mathbf{G}}(\underline{\mathbf{G}}^\top\underline{\mathbf{Q}}\underline{\mathbf{G}})^{-1}\underline{\mathbf{G}}^\top, \tag{4.5}$$

where $\underline{\mathbf{I}}$ denotes the identity matrix. The space of *admissible Lagrange multipliers* is given by

$$\boldsymbol{\Lambda}_{\mathrm{ad}} \;:=\; \ker(\underline{\mathbf{G}}^\top) \;=\; \mathrm{range}(\underline{\mathbf{P}}) \;=\; \{\boldsymbol{\lambda} \in \mathbb{R}^M : \underline{\mathbf{B}}^\top\boldsymbol{\lambda} \in \mathrm{range}(\underline{\mathbf{K}})\}. \tag{4.6}$$

The solution of system (4.1) is now performed according to Algorithm 1. For a derivation see, e.g., [17, 39, 35].

Apparently, the main effort lies in the solution of the dual equation:

$$\text{find } \widetilde{\boldsymbol{\lambda}} \in \boldsymbol{\Lambda}_{\mathrm{ad}} : \quad \underline{\mathbf{P}}^\top\underline{\mathbf{F}}\widetilde{\boldsymbol{\lambda}} \;=\; \underline{\mathbf{P}}^\top\underline{\mathbf{B}}\,\underline{\mathbf{K}}^\dagger(\mathbf{F} - \underline{\mathbf{B}}^\top\boldsymbol{\lambda}_0). \tag{4.7}$$

Since $\ker(\underline{\mathbf{B}}^\top) = \{0\}$ and $\mathrm{range}(\underline{\mathbf{P}}) = \boldsymbol{\Lambda}_{\mathrm{ad}}$, one can show that the system matrix $\underline{\mathbf{P}}^\top\underline{\mathbf{F}}$ is symmetric and positive definite on $\boldsymbol{\Lambda}_{\mathrm{ad}}$. Therefore, we use preconditioned conjugate gradients (PCG) to solve problem (4.7). Actually, the PCG algorithm can be acted out on the whole space $\mathbb{R}^M$, started with the initial vector $\boldsymbol{\lambda}_0$, see e.g. [39, Sect. 6.3]. The preconditioner in PCG has the form $\underline{\mathbf{P}}\,\underline{\mathbf{M}}^{-1}$, where $\underline{\mathbf{M}}^{-1}$ is specified below.

4.4. Choice of Preconditioner $\underline{\mathbf{M}}^{-1}$. Let us assume that Young's modulus E is constant in every subdomain:

$$E|_{\Omega^{(i)}} \;=\; E^{(i)} \;=\; \mathrm{const}. \tag{4.8}$$

This assumption can be weakened to the case that E is mildly varying in $\Omega^{(i)}$. In that case, we set $E^{(i)}$ to the maximum value of E on $\Omega^{(i)}$.

Let $\mathcal{E}^{(ij)} := \partial\Omega^{(i)} \cap \partial\Omega^{(j)}$ denote the subdomain edge shared by $\Omega^{(i)}$ and $\Omega^{(j)}$. If $\partial\Omega^{(i)} \cap \partial\Omega^{(j)}$ contains only a vertex, we simply set $\mathcal{E}^{(ij)} := \emptyset$. For each $j = 1, \ldots, N$ and each (non-trivial) subdomain edge $\mathcal{E}^{(ij)}$, we define

$$\delta^{(i)}_{\dagger,\mathcal{E}^{(ij)}} := \frac{(E^{(i)})^\gamma}{(E^{(i)})^\gamma + (E^{(j)})^\gamma}, \tag{4.9}$$

where $\gamma \in [1/2, \infty)$ is an exponent that can be chosen arbitrarily. By construction, $\delta^{(i)}_{\dagger,\mathcal{E}^{(ij)}} + \delta^{(j)}_{\dagger,\mathcal{E}^{(ij)}} = 1$. Furthermore, we have the elementary inequality

$$E^{(i)} \left(\delta^{(j)}_{\dagger,\mathcal{E}^{(ij)}}\right)^2 \le \min(E^{(i)}, E^{(j)}), \tag{4.10}$$

see [39, (6.19)] or [35, Lemma 2.98].

For each $i = 1, \ldots, N$ we define the diagonal matrix $\underline{\mathbf{D}}^{(i)} \in \mathbb{R}^{M\times M}$ as follows:

- for a coupling constraint on a subdomain edge $\mathcal{E}^{(ij)}$, we set the diagonal entry to $\delta^{(j)}_{\dagger,\mathcal{E}^{(ij)}}$,
- for a Dirichlet constraint on $\partial\Omega^{(i)}$, we set the diagonal entry to 1,
- all other entries are set to zero.

Using these scaling matrices, we define

$$\underline{\mathbf{B}}_D := [\underline{\mathbf{D}}^{(1)}\underline{\mathbf{B}}^{(1)} | \ldots | \underline{\mathbf{D}}^{(N)}\underline{\mathbf{B}}^{(N)}]. \tag{4.11}$$

Furthermore, let $\underline{\mathbf{S}}^{(i)} \in \mathbb{R}^{n^{(i)}\times n^{(i)}}$ denote the Schur complement of $\underline{\mathbf{K}}^{(i)}$ where all *interior dofs* are eliminated, filled up with zeros. For the sake of a simple presentation, assume that these dofs are ordered after all the others. Then $\underline{\mathbf{K}}^{(i)}$ and $\underline{\mathbf{S}}^{(i)}$ are of the form

$$\underline{\mathbf{K}}^{(i)} = \begin{bmatrix} \underline{\mathbf{K}}^{(i)}_{CC} & (\underline{\mathbf{K}}^{(i)}_{IC})^\top \\ \underline{\mathbf{K}}^{(i)}_{IC} & \underline{\mathbf{K}}^{(i)}_{II} \end{bmatrix}, \qquad \underline{\mathbf{S}}^{(i)} = \begin{bmatrix} \underline{\mathbf{K}}^{(i)}_{CC} - (\underline{\mathbf{K}}^{(i)}_{IC})^\top (\underline{\mathbf{K}}^{(i)}_{II})^{-1} \underline{\mathbf{K}}^{(i)}_{IC} & 0 \\ 0 & 0 \end{bmatrix}. \tag{4.12}$$

Let $\underline{\mathbf{S}} := \operatorname{diag}(\underline{\mathbf{S}}^{(i)})_{i=1}^N$, then the preconditioner $\underline{\mathbf{M}}^{-1}$ is defined by

$$\underline{\mathbf{M}}^{-1} := \underline{\mathbf{B}}_D \underline{\mathbf{S}} \underline{\mathbf{B}}_D^\top. \tag{4.13}$$

In the sequel, we refer to the above choice of $\underline{\mathbf{D}}^{(i)}$ by *coefficient scaling*. We speak of *multiplicity scaling*, if $\underline{\mathbf{D}}^{(i)}$ is constructed using $\delta^{(j)}_{\dagger,\mathcal{E}^{(ij)}} := 1/2$. In Sect. 6, we shall also use a *stiffness scaling*.

REMARK 4.1 (stiffness scaling). *Under the assumption that the meshes on $\Omega^{(i)}$ and $\Omega^{(j)}$ are quasi-uniform, that $\nu \ll 1/2$, and that one uses the dofs from Sect. 3.4, one may replace $E^{(i)}$ and $E^{(j)}$ in (4.9) by the maximum diagonal entry of $\underline{\mathbf{K}}^{(i)}$ resp. $\underline{\mathbf{K}}^{(j)}$ over the dofs on the subdomain edge $\mathcal{E}^{(ij)}$. The use of dof-wise weights $\delta^{(i)}_{\dagger,k}$ produced from the corresponding diagonal entries of the stiffness matrices is known to be problematic, in particular in the presence of ragged interfaces, cf. [23].*

4.5. Choice of $\underline{\mathbf{Q}}$. We propose to choose $\underline{\mathbf{Q}} = \underline{\mathbf{Q}}_{\text{diag}}$ as a diagonal matrix defined as follows. If the m-th Lagrange multiplier corresponds to a coupling pair $(i,k) \sim (j,\ell)$ of dofs, then

$$(\underline{\mathbf{Q}}_{\text{diag}})_{mm} := \frac{\min(E^{(i)}, E^{(j)})}{h^{(ij)}\, H^{(ij)}}, \tag{4.14}$$

where $H^{(ij)} = |\mathcal{E}^{(ij)}|$ denotes the length of subdomain edge $\mathcal{E}^{(ij)}$, and $h^{(ij)}$ is the maximal mesh size on $\mathcal{E}^{(ij)}$. We note that for the current choice of dofs, one can also set

$$(\underline{\mathbf{Q}}_{\text{diag}})_{mm} := \min(K^{(i)}_{kk}, K^{(j)}_{\ell\ell}) \frac{h^{(ij)}}{H^{(ij)}} \quad \text{or} \quad (\underline{\mathbf{Q}}_{\text{diag}})_{mm} := \frac{\min(K^{(i)}_{kk}, K^{(j)}_{\ell\ell})}{\#\text{ dofs on } \mathcal{E}^{(ij)}},$$

where $K^{(i)}_{kk}$ is the diagonal entry of $\underline{\mathbf{K}}^{(i)}$ at k. If Assumption 5.13 and Assumption 5.23 below hold, then all three expressions above turn out to be equivalent. In variant (b), if the m-th Lagrange multiplier corresponds to a Dirichlet dof $(i,k) \sim \Gamma_D$, then

$$(\underline{\mathbf{Q}}_{\text{diag}})_{mm} := \frac{E^{(i)}}{h^{(iD)} H^{(iD)}}, \tag{4.15}$$

with $H^{(iD)} := |\partial\Omega^{(i)} \cap \Gamma_D|$ and $h^{(iD)}$ the maximal mesh size on $\partial\Omega \cap \Gamma_D$. Obviously, $\underline{\mathbf{Q}}_{\text{diag}}$ is positive definite and so the projection $\underline{\mathbf{P}}$ in (4.5) is well-defined. Let us note that formulae (4.14)–(4.15) hold for the choice of dofs from Sect. 3.4; if the dofs scale differently, one has to modify $\underline{\mathbf{Q}}_{\text{diag}}$ accordingly.

REMARK 4.2. *From* (4.5) *and Algorithm 1, one sees that the algorithm remains invariant if* $\underline{\mathbf{Q}}$ *is scaled by a global (positive) factor. Hence (i) if Young's modulus* E *is globally constant, then* $E^{(i)}$, $E^{(j)}$ *in* (4.14)–(4.14) *may be replaced by* 1, *(ii) if the global mesh and the subdomain partition are quasi-uniform, then* $h^{(ij)}H^{(i)}$, $h^{(iD)}H^{(i)}$ *in* (4.14)–(4.14) *may be replaced by* 1. *If both conditions hold, we can simply use* $\underline{\mathbf{Q}} = \underline{\mathbf{I}}$.

REMARK 4.3. *As frequently proposed in the literature, one can also use* $\underline{\mathbf{Q}} = \underline{\mathbf{M}}^{-1}$, *provided that* $\underline{\mathbf{M}}^{-1}$ *is positive definite on* range($\underline{\mathbf{G}}$), *which is always true in variant (a). In variant (b), the matrix* $\underline{\mathbf{G}}^\top \underline{\mathbf{Q}} \underline{\mathbf{G}}$ *may become singular. A simple remedy is to select in each subdomain enough interior dofs, such that the rigid body modes are fixed. These special dofs are then added to the* C*-block in* (4.12) *(and thus* not *eliminated in the Schur complement* $\underline{\mathbf{S}}_i$*). In our 2D case, one can, e.g., take all dofs associated to an interior edge. If this interior edge is in the subdomain center (with distance* $\mathcal{O}(H)$ *from the interface), then the analysis below is still valid.*

5. Analysis.

5.1. Abstract Framework. Following the abstract framework summarized, e.g., in [39], we define

$$\underline{\mathbf{P}}_D := \underline{\mathbf{B}}_D^\top \underline{\mathbf{B}}, \qquad \underline{\mathbf{E}}_D := \underline{\mathbf{I}} - \underline{\mathbf{P}}_D\,. \tag{5.1}$$

Without major effort, one can show that for a block vector $\mathbf{W} = [\mathbf{W}^{(1)\top} | \dots | \mathbf{W}^{(N)\top}]^\top$,

$$(\underline{\mathbf{P}}_D \mathbf{W})^{(i)}_k = \begin{cases} \delta^{(j)}_{\dagger,\mathcal{E}^{(ij)}} \left(W^{(i)}_k - W^{(j)}_\ell\right) & \text{if } (i,k) \sim (j,\ell) \text{ on } \mathcal{E}^{(ij)}\,, \\ W^{(i)}_k & \text{if } (i,k) \sim \Gamma_D\,, \\ 0 & \text{else.} \end{cases} \tag{5.2}$$

It is then easily seen that

$$\underline{\mathbf{B}}\,\underline{\mathbf{M}}^{-1}\underline{\mathbf{B}}^\top = \underline{\mathbf{P}}_D^\top \underline{\mathbf{S}}\,\underline{\mathbf{P}}_D\,, \qquad \underline{\mathbf{B}}\,\underline{\mathbf{P}}_D = \underline{\mathbf{B}}. \tag{5.3}$$

From the last identity, we see that $\underline{\mathbf{P}}_D$ and $\underline{\mathbf{E}}_D$ are projections. In range($\underline{\mathbf{P}}_D$), all interior dofs vanish. Conversely, in range($\underline{\mathbf{E}}_D$), all coupling dofs are continuous and the homogeneous Dirichlet conditions are fulfilled.

The next lemma ensures that the preconditioner $\underline{\mathbf{P}}\,\underline{\mathbf{M}}^{-1}$ is positive definite on the subspace $\mathbf{\Lambda}_{\mathrm{ad}}$ where the PCG iteration takes place.

LEMMA 5.1. *Provided that* $\underline{\mathbf{Q}}$ *is definite on* $\mathrm{range}(\underline{\mathbf{G}})$*, the operator* $\underline{\mathbf{P}}\,\underline{\mathbf{M}}^{-1}$ *is SPD on* $\mathbf{\Lambda}_{\mathrm{ad}}$*.*

Proof. See, e.g., [35, Lemma 2.43] or [39, Lemma 6.11, Lemma 6.18]. ∎

As a next step, one reduces the condition number bound to a single stability estimate of the operator $\underline{\mathbf{P}}_D$, see (5.4) below. Before, we need to introduce a couple of function and vector spaces.

DEFINITION 5.2.

(i) We say that $\Omega^{(i)}$ *is* non-floating *if* $\ker(\underline{\mathbf{K}}^{(i)}) = \{0\}$*, and otherwise* floating*. In variant (a), the non-floating subdomains are exactly those where* $\partial\Omega^{(i)} \cap \Gamma_D$ *has positive surface measure, in variant (b) all subdomains are floating. If* $\Omega^{(i)}$ *is floating,* $\ker(\underline{\mathbf{K}}^{(i)})$ *corresponds to the space of (infinitesimal) rigid body motions,*

$$\mathcal{RB} := \{\mathbf{a} + b\,[-x_2, x_1]^\top : \mathbf{a} \in \mathbb{R}^2,\, b \in \mathbb{R}\}.$$

(ii) Let $\mathbb{W}^{(i)} \subset \mathbb{R}^{n^{(i)}}$ *be the subspace of vectors* $\mathbf{W}^{(i)}$ *such that*

$$\underline{\mathbf{K}}_{IC}^{(i)}\mathbf{W}_C^{(i)} + \underline{\mathbf{K}}_{II}^{(i)}\mathbf{W}_I^{(i)} \;=\; 0$$

and let $\mathcal{W}^{(i)} \subset \mathbf{V}_h^{(i)} \times \overline{V}_{n,h}^{(i)}$ *be the corresponding space of discrete PDE-harmonic functions.*

(iii) We define

$$\mathcal{W}^{(i),\perp} := \begin{cases} \{(\mathbf{v}, \overline{v}_n) \in \mathcal{W}^{(i)} : \int\limits_{\Omega^{(i)}} \mathbf{v}\cdot\mathbf{z}\,dx = 0 \quad \forall \mathbf{z} \in \mathcal{RB}\} & \text{if } \Omega^{(i)} \text{ is floating,} \\ \mathcal{W}^{(i)} & \text{else,} \end{cases}$$

and let $\mathbb{W}^{(i),\perp}$ *denote the corresponding subspace of* $\mathbb{R}^{n^{(i)}}$*.*

(iv) We set $\mathbb{W} := \prod_{i=1}^N \mathbb{W}^{(i)}$ *and* $\mathcal{W} := \prod_{i=1}^N \mathcal{W}^{(i)}$*, and define* $\mathbb{W}^\perp$*,* $\mathcal{W}^\perp$ *in the analogous manner.*

(v) We define the semi-norm $|\mathbf{W}|_{\underline{\mathbf{S}}}$ *on* $\mathbb{W}$ *by*

$$|\mathbf{W}|_{\underline{\mathbf{S}}} := \Big(\sum_{i=1}^N (\mathbf{W}^{(i)})^\top \underline{\mathbf{S}}^{(i)} \mathbf{W}^{(i)}\Big)^{1/2}.$$

On $\mathbb{W}^\perp$*, this becomes actually a norm.*

LEMMA 5.3. *For any* $\mathbf{W} \in \mathbb{W}$*, there exists a unique element* $\mathbf{Z}_{\mathbf{W}} \in \ker(\underline{\mathbf{K}})$ *such that* $\underline{\mathbf{B}}(\mathbf{W} + \mathbf{Z}_{\mathbf{W}}) \in \mathbf{\Lambda}_{\mathrm{ad}}$*. Moreover, if* $\underline{\mathbf{Q}}$ *is SPD on* $\mathbf{\Lambda}_{\mathrm{ad}}$*, then* $\|\underline{\mathbf{B}}\mathbf{Z}_{\mathbf{W}}\|_{\underline{\mathbf{Q}}} \le \|\underline{\mathbf{B}}\mathbf{W}\|_{\underline{\mathbf{Q}}}$*, where* $\|\boldsymbol{\lambda}\|_{\underline{\mathbf{Q}}} = (\boldsymbol{\lambda}^\top \underline{\mathbf{Q}}\boldsymbol{\lambda})^{1/2}$*.*

Proof. See [39, Lemma 6.19], $\mathbf{Z}_{\mathbf{W}} = -\underline{\mathbf{R}}(\underline{\mathbf{G}}\underline{\mathbf{Q}}^\top\underline{\mathbf{G}})^{-1}\underline{\mathbf{G}}^\top\underline{\mathbf{Q}}\underline{\mathbf{B}}\mathbf{W}$. ∎

LEMMA 5.4. *Let* ω *be such that*

$$|\underline{\mathbf{P}}_D(\mathbf{W} + \mathbf{Z}_{\mathbf{W}})|_{\underline{\mathbf{S}}}^2 \;\le\; \omega\,|\mathbf{W}|_{\underline{\mathbf{S}}}^2 \qquad \forall \mathbf{W} \in \mathbb{W}^\perp, \tag{5.4}$$

where $\mathbf{Z}_{\mathbf{W}}$ *is the element from Lemma 5.3. Then*

$$\kappa(\underline{\mathbf{P}}\,\underline{\mathbf{M}}^{-1}\underline{\mathbf{P}}^\top\underline{\mathbf{F}}_{|\mathbf{\Lambda}_{\mathrm{ad}}}) \;\le\; \omega.$$

Proof. See, e.g., [39, Sect. 6.3] or [35, Lemma 2.45, Lemma 2.103]. ∎

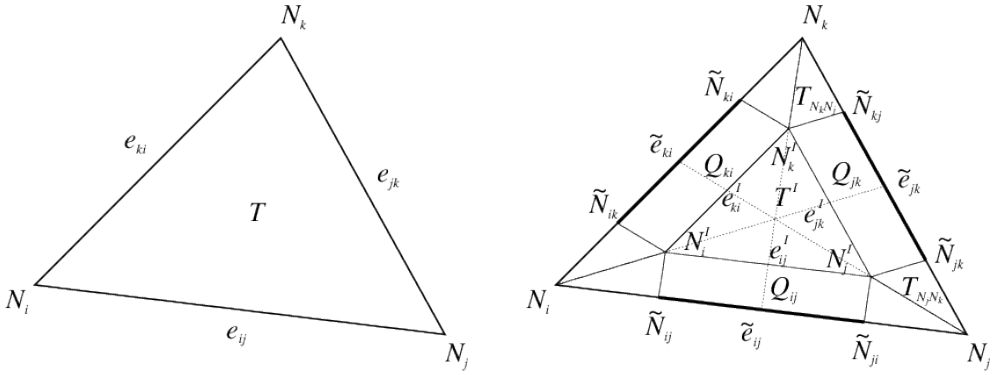

FIG. 5.1. *Refinement of triangle $T \in \mathcal{T}_h$ into triangles and quadrilaterals.*

5.2. Transformation to Conforming Finite Elements. In this subsection, we develop a transformation $\mathcal{X}^{(i)}$ from the TDNNS space $\mathbf{V}_h^{(i)} \times \overline{V}_{n,h}^{(i)}$ to the usual finite element space of continuous and piecewise linear elements on a refined mesh. Additionally, we provide an "inverse" transformation $\mathcal{Y}^{(j)}$ mapping continuous finite element functions back to the original TDNNS space. As an essential property, both operators preserve the rigid body motions. Furthermore, we derive several stability estimates in the respective H^1 and L^2 norms. The following auxiliary lemma will be needed a couple of times.

LEMMA 5.5. *Let K be a triangle/quadrilateral of a shape-regular mesh, such that the affine (bi)linear map $F_K : \widehat{K} \to K$ from the reference triangle/quadrilateral to K satisfies $\|\nabla F_K\| \simeq h_K$ and $\det(\nabla F_K) \simeq h_K^2$, where $h_K = \operatorname{diam}(K)$. Let $\mathcal{V}_K = \{N_i\}$ denote the set of vertices K and $\mathcal{E}_K = \{e_{ij}\}$ the set of edges, such that N_i, N_j are the end points of edge e_{ij}. Then, for any (bi)linear function $\mathbf{v} : K \to \mathbb{R}^2$,*

$$\|\mathbf{v}\|^2_{\mathbf{L}^2(K)} \simeq h_K^2 \sum_{N \in \mathcal{V}_K} |\mathbf{v}(N)|^2, \tag{5.5}$$

$$\|\nabla \mathbf{v}\|^2_{\mathbf{L}^2(Q)} \simeq \sum_{e_{ij} \in \mathcal{E}_K} |\mathbf{v}(N_i) - \mathbf{v}(N_j)|^2. \tag{5.6}$$

The constants of equivalence depend only on the (bi)linear mapping F_K.

Proof. The result is obtained by transformation to the reference element. ∎

The next definition specifies the refined mesh.

DEFINITION 5.6 (Refinement of triangle). *As indicated in Figure 5.1, each triangle T of the mesh $\mathcal{T}_h$ is decomposed into several triangles and quadrilaterals. For $i \neq j \neq k \in \{1, 2, 3\}$, define the following nodal points:*

- *the nodes N_i of the original triangle T,*
- *the nodes $N_i^I = \frac{2}{3}N_i + \frac{1}{6}(N_j + N_k)$ interior to the triangle,*
- *the nodes $\tilde{N}_{jk} = \frac{3}{4}N_j + \frac{1}{4}N_k$ on the triangle edges*

The triangular element T shall be decomposed into

- *an inner triangle T^I with nodes N_i^I and edges $e_{jk}^I = \overline{N_j^I N_k^I}$, such the barycenters of T and T^I coincide and $|T^I| = \frac{1}{4}|T|$,*
- *three parallelograms Q_{jk} with nodes N_j^I, N_k^I, $\tilde{N}_{jk}$, $\tilde{N}_{kj}$, and the parallel edges e_{jk}^I and $\tilde{e}_{jk} = \overline{\tilde{N}_{jk}\tilde{N}_{kj}}$,*
- *six triangles $T_{N_iN_j}$ for $i \neq j$ with nodes N_i, N_i^I, $\tilde{N}_{ij}$.*

This refinement leads to a globally conforming hybrid triangular-quadrilateral mesh $\mathcal{T}_h^{ref}$. If $\mathcal{T}_h$ is shape-regular, then $\mathcal{T}_h^{ref}$ is shape-regular as well.

DEFINITION 5.7. *Let $\hat{\mathbf{V}}_h^{(i)} \subset \mathbf{H}^1(\Omega^{(i)})$ denote the space of globally continuous vector-valued functions, that are piecewise (bi)linear with respect to the refined mesh $\mathcal{T}_h^{ref,(i)}$ from Definition 5.6. The operator*

$$\mathcal{X}^{(i)} : \mathbf{V}_h^{(i)} \times \overline{V}_{n,h}^{(i)} \to \hat{\mathbf{V}}_h^{(i)} : (\mathbf{v}^{(i)}, \overline{v}_n^{(i)}) \mapsto \hat{\mathbf{v}}^{(i)}$$

is defined by prescribing the values of $\hat{\mathbf{v}}^{(i)}$ at the nodes of $\mathcal{T}_h^{ref,(i)}$ as follows.

(i) For the nodes N_j^I of T^I (see Definition 5.6), we set

$$\hat{\mathbf{v}}(N_j^I) := \mathbf{v}(N_j^I).$$

By construction, $\hat{\mathbf{v}}^{(i)} = \mathbf{v}^{(i)}$ on T^I for all elements $T \in \mathcal{T}_h^{(i)}$.

(ii) For the nodes $\tilde{N}_{k\ell}$, $\tilde{N}_{\ell k}$ on the edge part $\tilde{e}_{k\ell}$, we set

$$\hat{\mathbf{v}}^{(i)}(\tilde{N}_{k\ell}) := \mathbf{v}_t^{(i)}(\tilde{N}_{k\ell}) + \overline{v}_n^{(i)}(\tilde{N}_{k\ell})\mathbf{n}, \qquad \hat{\mathbf{v}}^{(i)}(\tilde{N}_{\ell k}) := \mathbf{v}_t^{(i)}(\tilde{N}_{\ell k}) + \overline{v}_n^{(i)}(\tilde{N}_{\ell k})\mathbf{n},$$

where $\mathbf{n}$ is the unit normal vector to edge $e_{k\ell}$ (with globally fixed orientation), and $\mathbf{v}_t^{(i)}$ is the corresponding (continuous) tangential component of $\mathbf{v}^{(i)}$ on $e_{k\ell}$.

(iii) To define the values at the nodes N_j of the original mesh $\mathcal{T}_h^{(i)}$, we average the (discontinuous) function $\mathbf{v}^{(i)}$:

$$\hat{\mathbf{v}}^{(i)}(N_j) := \frac{1}{\#\{T : N_j \in T\}} \sum_{T : N_j \in T} (\mathbf{v}_{|T}^{(i)})(N_j).$$

Apparently, the finite element function $\hat{\mathbf{v}}^{(i)}$ is well-defined, piecewise (bi)linear with respect to $\mathcal{T}_h^{ref,(i)}$, and continuous on subdomain $\Omega^{(i)}$. Moreover, if $\mathbf{v}^{(i)}$ is a continuous function and $\overline{v}_n^{(i)}$ its normal component, then $\hat{\mathbf{v}}^{(i)} = \mathbf{v}^{(i)}$. Consequently, the operator $\mathcal{X}^{(i)}$ preserves rigid body transformations on $\Omega^{(i)}$.

LEMMA 5.8. *For the operator $\mathcal{X}^{(i)}$ from Definition 5.7 and any TDNNS finite element function $(\mathbf{v}^{(i)}, \overline{v}_n^{(i)}) \in \mathbf{V}_h^{(i)} \times \overline{V}_{n,h}^{(i)}$ with continuous counterpart $\hat{\mathbf{v}}^{(i)} = \mathcal{X}^{(i)}(\mathbf{v}^{(i)}, \overline{v}_n^{(i)})$,*

$$|\mathbf{v}^{(i)}, \overline{v}_n^{(i)}|_{\mathbf{H}^1(\Omega^{(i)}, \mathcal{T}_h^{(i)})} \;\simeq\; |\hat{\mathbf{v}}^{(i)}|_{\mathbf{H}^1(\Omega^{(i)})}. \tag{5.7}$$

Proof. Throughout the proof, all references to the subdomain index (i) are omitted. The equivalence is shown element-wise, where on each element the different parts T_I, Q_{jk} and $T_{N_j N_k}$ are considered separately.

Inner part T^I of element T. Since the gradient $\nabla \mathbf{v} = \nabla \hat{\mathbf{v}}$ is constant and $|T| = 4\,|T^I|$,

$$|\mathbf{v}|^2_{\mathbf{H}^1(T)} \;=\; 4\,|\hat{\mathbf{v}}|^2_{\mathbf{H}^1(T^I)}. \tag{5.8}$$

Quadrilateral part Q_{jk} of element T. From Lemma 5.5 we know that

$$
\begin{aligned}
|\hat{\mathbf{v}}|^2_{\mathbf{H}^1(Q_{jk})} \;\simeq\; & |\hat{\mathbf{v}}(N_j^I) - \hat{\mathbf{v}}(N_k^I)|^2 + |\hat{\mathbf{v}}(\tilde{N}_{kj}) - \hat{\mathbf{v}}(\tilde{N}_{jk})|^2 + \\
& |\hat{\mathbf{v}}(N_k^I) - \hat{\mathbf{v}}(\tilde{N}_{kj})|^2 + |\hat{\mathbf{v}}(N_j^I) - \hat{\mathbf{v}}(\tilde{N}_{jk})|^2
\end{aligned} \tag{5.9}
$$

A geometrical consideration gives for $i \neq j \neq k$

$$
\hat{\mathbf{v}}(N_j^I) = \tfrac{2}{3}\mathbf{v}(N_j) + \tfrac{1}{6}\left(\mathbf{v}(N_k) + \mathbf{v}(N_i)\right), \tag{5.10}
$$

$$
\hat{\mathbf{v}}(\tilde{N}_{jk}) = \left(\tfrac{3}{4}\mathbf{v}_t(N_j) + \tfrac{1}{4}\mathbf{v}_t(N_k)\right) + \left(\tfrac{3}{4}\overline{v}_n(N_j) + \tfrac{1}{4}\overline{v}_n(N_k)\right)\mathbf{n}, \tag{5.11}
$$

where $\mathbf{n}$ is the normal vector on edge e_{jk}. Now we compute the different terms on the right-hand side of (5.9). For first and second term, corresponding to the parallel edges e^I_{jk} and $\tilde{e}_{jk}$, we obtain

$$
|\hat{\mathbf{v}}(N_j^I) - \hat{\mathbf{v}}(N_k^I)|^2 = \tfrac{1}{4}\left|(\mathbf{v}(N_j) - \mathbf{v}(N_k))\right|^2, \tag{5.12}
$$

$$
|\hat{\mathbf{v}}(\tilde{N}_{kj}) - \hat{\mathbf{v}}(\tilde{N}_{jk})|^2 = \tfrac{1}{4}\left(\left|(\mathbf{v}_t(N_k) - \mathbf{v}_t(N_j))\right|^2 + \left(\overline{v}_n(N_k) - \overline{v}_n(N_j)\right)^2\right). \tag{5.13}
$$

In (5.13), the orthogonality of normal and tangential component has been used. The third and fourth term of (5.9) are of the same structure. We insert (5.10), (5.11) for $\hat{\mathbf{v}}$, split $\mathbf{v} = \mathbf{v}_t + v_n\mathbf{n}$ into tangential and normal component with respect to the edge normal $\mathbf{n} = \mathbf{n}_{e_{jk}}$, and treat the orthogonal parts separately. By definition of $\hat{\mathbf{v}}$, we see

$$
\begin{aligned}
\hat{\mathbf{v}}(N_k^I) - \hat{\mathbf{v}}(\tilde{N}_{kj}) = \; & \tfrac{1}{12}\left[2\mathbf{v}(N_i) - \mathbf{v}(N_k) - \mathbf{v}(N_j)\right] \\
& + \left[\tfrac{3}{4}(v_n(N_k) - \overline{v}_n(N_k)) + \tfrac{1}{4}(v_n(N_j) - \overline{v}_n(N_j))\right]\mathbf{n}.
\end{aligned} \tag{5.14}
$$

It is clear to see from this decomposition the upper bound

$$
\begin{aligned}
& |\hat{\mathbf{v}}(N_k^I) - \hat{\mathbf{v}}(\tilde{N}_{kj})|^2 + |\hat{\mathbf{v}}(N_j^I) - \hat{\mathbf{v}}(\tilde{N}_{jk})|^2 \\
& \lesssim (v_n(N_j) - \overline{v}_n(N_j))^2 + (v_n(N_k) - \overline{v}_n(N_k))^2 + \sum_{\ell \neq m} |\mathbf{v}(N_\ell) - \mathbf{v}(N_m)|^2 \\
& \lesssim |\mathbf{v}, \overline{v}_n|^2_{\mathbf{H}^1(T,\mathcal{T}_h)},
\end{aligned} \tag{5.15}
$$

where in the last step, we have used Lemma 5.5.

To get a lower bound, it is necessary to add the H^1 semi-norm of $\hat{\mathbf{v}}$ on the inner triangle T^I. Then it follows from a straightforward but tedious algebraic computation that, for any positive constant κ, there exists some positive $c(\kappa) > 0$ with,

$$
\begin{aligned}
& |\hat{\mathbf{v}}(N_k^I) - \hat{\mathbf{v}}(\tilde{N}_{kj})|^2 + |\hat{\mathbf{v}}(N_j^I) - \hat{\mathbf{v}}(\tilde{N}_{jk})|^2 + \kappa\,|\hat{\mathbf{v}}|^2_{\mathbf{H}^1(T^I)} \\
& \simeq |\hat{\mathbf{v}}(N_k^I) - \hat{\mathbf{v}}(\tilde{N}_{kj})|^2 + |\hat{\mathbf{v}}(N_j^I) - \hat{\mathbf{v}}(\tilde{N}_{jk})|^2 + \sum_{\ell \neq m} |\hat{\mathbf{v}}(N_\ell) - \hat{\mathbf{v}}(N_m)|^2 \\
& \gtrsim c(\kappa)\left((v_n(N_j) - \overline{v}_n(N_j))^2 + (v_n(N_k) - \overline{v}_n(N_k))^2\right).
\end{aligned} \tag{5.16}
$$

Combining (5.9) with (5.12)–(5.16), and choosing $\kappa = 1/6$ we see that

$$
\begin{aligned}
& (v_n(N_j) - \overline{v}_n(N_j))^2 + (v_n(N_k) - \overline{v}_n(N_k))^2 \\
& \qquad \lesssim \; |\hat{\mathbf{v}}|^2_{\mathbf{H}^1(Q_{jk})} + \tfrac{1}{6}|\hat{\mathbf{v}}|^2_{\mathbf{H}^1(T^I)} \\
& \qquad \lesssim \; \sum_{\ell \neq m} |\mathbf{v}(N_\ell) - \mathbf{v}(N_m)|^2 + \left(\overline{v}_n(N_k) - \overline{v}_n(N_j)\right)^2 \\
& \qquad\qquad + \left(v_n(N_j) - \overline{v}_n(N_j)\right)^2 + \left(v_n(N_k) - \overline{v}_n(N_k)\right)^2.
\end{aligned} \tag{5.17}
$$

A triangle inequality argument allows to remove $\big(\overline{v}_n(N_k) - \overline{v}_n(N_j)\big)^2$ in the upper bound. Transformation to the reference edge yields

$$(v_n(N_j) - \overline{v}_n(N_j))^2 + (v_n(N_k) - \overline{v}_n(N_k))^2 \simeq h^{-1}\|v_n - \overline{v}_n\|^2_{L^2(e_{jk})}, \tag{5.18}$$

and together with Lemma 5.5 we arrive at

$$h^{-1}\|v_n - \overline{v}_n\|^2_{L^2(e_{jk})} \lesssim |\hat{\mathbf{v}}|^2_{\mathbf{H}^1(Q_{jk})} + \tfrac{1}{6}|\hat{\mathbf{v}}|^2_{\mathbf{H}^1(T^I)} \lesssim |\mathbf{v}|^2_{\mathbf{H}^1(T)} + h^{-1}\|v_n - \overline{v}_n\|^2_{L^2(e_{jk})}. \tag{5.19}$$

Triangles $T_{N_jN_k}$ attached to node N_j. Let $\mathcal{N}(N_j)$ be the set of nodes in $\mathcal{T}_h$ that are linked by an edge with N_j, and let $\mathcal{T}(e_{j\ell})$ denotes the set of elements attached to edge $e_{j\ell}$. In this paragraph, we show that

$$\begin{aligned} 0 &\le |\hat{\mathbf{v}}|^2_{\mathbf{H}^1(T_{N_jN_k})} \\ &\lesssim |\mathbf{v},\, \overline{v}_n|^2_{\mathbf{H}^1(T,\mathcal{T}_h)} + \sum_{N_\ell \in \mathcal{N}(N_j)} \sum_{T' \in \mathcal{T}(e_{j\ell})} h^{-1}\, \|\mathbf{v}_{|T'} \cdot \mathbf{n} - \overline{v}_n\|^2_{L^2(e_{j\ell})}\,, \end{aligned} \tag{5.20}$$

where the lower bound is trivial. An application of Lemma 5.5 yields

$$|\hat{\mathbf{v}}|^2_{\mathbf{H}^1(T_{N_jN_k})} \eqsim |\hat{\mathbf{v}}(\tilde{N}_{jk}) - \hat{\mathbf{v}}(N_j^I)|^2 + |\hat{\mathbf{v}}(N_j^I) - \hat{\mathbf{v}}(N_j)|^2 + |\hat{\mathbf{v}}(N_j) - \hat{\mathbf{v}}(\tilde{N}_{jk})|^2\,. \tag{5.21}$$

As shown previously, the first term on the right-hand side is $\lesssim |\mathbf{v},\, \overline{v}_n|^2_{\mathbf{H}^1(T,\mathcal{T}_h)}$. For the second term, we use a triangle inequality and employ the definition of $\hat{\mathbf{v}}(N_j)$ as a mean value:

$$\begin{aligned} |\hat{\mathbf{v}}(N_j^I) - \hat{\mathbf{v}}(N_j)|^2 &\lesssim |\mathbf{v}_{|T}(N_j^I) - \mathbf{v}_{|T}(N_j)|^2 + \big|\mathbf{v}_{|T}(N_j) - \frac{1}{\#\mathcal{T}_j}\sum_{T' \in \mathcal{T}_j} \mathbf{v}_{|T'}(N_j)\big|^2 \\ &\lesssim |\mathbf{v}_{|T}(N_j^I) - \mathbf{v}_{|T}(N_j)|^2 + \sum_{T' \in \mathcal{T}_j} |\mathbf{v}_{|T}(N_j) - \mathbf{v}_{|T'}(N_j)|^2, \end{aligned}$$

where $\mathcal{T}_j := \{T' \in \mathcal{T}_h : N_j \in T'\}$. Repetitive application of the triangle inequality allows an upper bound of the form

$$|\mathbf{v}_{|T}(N_j^I) - \mathbf{v}_{|T}(N_j)|^2 + \sum_{N_\ell \in \mathcal{N}(N_j)} \big|\mathbf{v}_{|T_{e_{j\ell},1}}(N_j) - \mathbf{v}_{|T_{e_{j\ell},2}}(N_j)\big|^2\,,$$

where $T_{e_{j\ell},1}$, $T_{e_{j\ell},2}$ denote the two elements attached to the edge $e_{j\ell}$. On $e_{j\ell}$, the tangential component of $\mathbf{v}$ is continuous, so the last difference above can be rewritten using the normal jump only. Finally, Lemma 5.5, transformation to the reference edge (like in (5.18)), and the triangle inequality (inserting $\overline{v}_n$) lead to the upper bound in (5.20). The third term in (5.21) is treated analogously.

Final estimate. Collecting the estimates (5.8), (5.19), and (5.20) on the different parts of $|\hat{\mathbf{v}}|_{H^1(\Omega)}$, summing over the elements and nodes of $\mathcal{T}_h$, and using the shape regularity of $\mathcal{T}_h$, we arrive at the desired result

$$|\hat{\mathbf{v}}|^2_{\mathbf{H}^1(\Omega)} \simeq \sum_{T \in \mathcal{T}_h} \Big(|\mathbf{v}|^2_{\mathbf{H}^1(T)} + h^{-1}\|v_n - \overline{v}_n\|^2_{L^2(\partial T)}\Big) = |\mathbf{v}, \overline{v}_n|^2_{\mathbf{H}^1(\Omega,\mathcal{T}_h)}. \tag{5.22}$$

This concludes the proof of Lemma 5.8. □

The following lemma discusses the L^2-stability of the operator $\mathcal{X}^{(i)}$.

LEMMA 5.9. *Let* $(\mathbf{v}^{(i)}, \overline{v}_n^{(i)}) \in \mathbf{V}_h^{(i)} \times \overline{V}_{n,h}^{(i)}$ *and* $\hat{\mathbf{v}}^{(i)} = \mathcal{X}^{(i)}(\mathbf{v}^{(i)}, \overline{v}_n^{(i)})$. *Then for each* $T \in \mathcal{T}_h^{(i)}$,

$$\|\mathbf{v}^{(i)}\|^2_{\mathbf{L}^2(T)} + h\|\overline{v}_n^{(i)}\|^2_{L^2(\partial T)} \lesssim \|\hat{\mathbf{v}}^{(i)}\|^2_{\mathbf{L}^2(T)} \lesssim \|\mathbf{v}^{(i)}\|^2_{\mathbf{L}^2(\omega_T)} + h\|\overline{v}_n^{(i)}\|^2_{L^2(\partial T)}, \tag{5.23}$$

where $\omega_T := \bigcup\{T' \in \mathcal{T}_h^{(i)} : T \cap T' \neq \emptyset\}$ *is the element-patch of* T. *Consequently,*

$$\|\hat{\mathbf{v}}^{(i)}\|^2_{\mathbf{L}^2(\Omega^{(i)})} \simeq \|\mathbf{v}^{(i)}\|^2_{\mathbf{L}^2(\Omega^{(i)})} + \sum_{T \in \mathcal{T}_h^{(i)}} h\,\|\overline{v}_n^{(i)}\|^2_{L^2(\partial T)}. \tag{5.24}$$

Proof. The proof works along the same lines as the proof of Lemma 5.8, using the L^2-norm equivalence (5.5). ∎

To show quasi-optimality of the FETI method, we also need operators $\mathcal{Y}^{(i)}$, which are kind of inverse to $\mathcal{X}^{(i)}$ and generate a discontinuous TDNNS pair $(\mathbf{v}^{(i)}, \overline{v}_n^{(i)})$ on the original triangulation $\mathcal{T}_h^{(i)}$ when applied to a continuous function $\hat{\mathbf{v}}^{(i)}$. Also for these operators, L^2 and H^1 stability estimates are provided.

DEFINITION 5.10. *Let* $\mathbf{V}_h^{(i)} \times \overline{V}_{n,h}^{(i)}$ *be the TDNNS finite element space on the subdomain mesh* $\mathcal{T}_h^{(i)}$. *Let* $\hat{\mathbf{V}}_h^{(i)}$ *be the standard* H^1 *conforming space of piecewise (bi)linear functions on the refined mesh* $\mathcal{T}_h^{ref,(i)}$. *We define the operator*

$$\mathcal{Y}^{(i)} : \hat{\mathbf{V}}_h^{(i)} \to \mathbf{V}_h^{(i)} \times \overline{V}_{n,h}^{(i)} : \hat{\mathbf{v}}^{(i)} \mapsto (\mathbf{v}^{(i)}, \overline{v}_n^{(i)})$$

locally using the decomposition from Definition 5.6:

- *for each triangle* T, *the function* $\mathbf{v}^{(i)}|_T \in \mathbf{P}^1$ *is chosen such that*

$$\mathbf{v}_t^{(i)} = \hat{\mathbf{v}}_t^{(i)} \qquad \text{on } \tilde{e}_{jk}, \tag{5.25}$$

  for each of the three edge parts $\tilde{e}_{jk}$ *(this defines* $\mathbf{v}^{(i)}|_T$ *uniquely by its Nédélec dofs).*
- *for each edge* e_{jk} *with normal vector* $\mathbf{n}$, *the function* $\overline{v}_n^{(i)}$ *is chosen as the linear extension of* $\hat{v}_n^{(i)} = \hat{\mathbf{v}}^{(i)} \cdot \mathbf{n}$ *from* $\tilde{e}_{jk}$ *to* e_{jk}, *such that*

$$\overline{v}_n^{(i)} = \hat{v}_n^{(i)} \qquad \text{on } \tilde{e}_{jk}. \tag{5.26}$$

The resulting function $(\mathbf{v}^{(i)}, \overline{v}_n^{(i)})$ *is well-defined and indeed in* $\mathbf{V}_h^{(i)} \times \overline{V}_{n,h}^{(i)}$. *If* $\hat{\mathbf{v}}^{(i)}$ *is piecewise linear on the initial mesh* $\mathcal{T}_h^{(i)}$, *then* $\mathbf{v}^{(i)} = \hat{\mathbf{v}}^{(i)}$ *and* $\overline{v}_n^{(i)} = \hat{v}_n^{(i)}$ *on all edges* e_{jk}. *In particular, the operator* $\mathcal{Y}^{(i)}$ *preserves rigid body transformations.*

LEMMA 5.11. *Let* $\hat{\mathbf{v}}^{(i)} \in \hat{\mathbf{V}}_h^{(i)}$ *and* $(\mathbf{v}^{(i)}, \overline{v}_n^{(i)}) := \mathcal{Y}^{(i)}\hat{\mathbf{v}}^{(i)}$. *Then for each* $T \in \mathcal{T}_h^{(i)}$,

$$\|\mathbf{v}^{(i)}\|^2_{\mathbf{L}^2(T)} + h\|\overline{v}_n^{(i)}\|^2_{L^2(\partial T)} \lesssim \|\hat{\mathbf{v}}^{(i)}\|^2_{\mathbf{L}^2(T)}. \tag{5.27}$$

In particular,

$$\|\mathbf{v}^{(i)}\|^2_{\mathbf{L}^2(\Omega^{(i)})} + \sum_{T \in \mathcal{T}_h^{(i)}} h\|\overline{v}_n^{(i)}\|^2_{L^2(\partial T)} \lesssim \|\hat{\mathbf{v}}^{(i)}\|^2_{\mathbf{L}^2(\Omega^{(i)})}. \tag{5.28}$$

Proof. As in the proof of Lemma 5.8, all reference to the subdomain index (i) shall be omitted. Since the tangential components $\mathbf{v}_t(\tilde{N}_{jk}) = \hat{\mathbf{v}}_t(\tilde{N}_{jk})$ coincide, one immediately sees by transformation to the reference element and Lemma 5.5

$$\|\mathbf{v}\|^2_{\mathbf{L}^2(T)} \;\simeq\; \sum_{e_{jk}\subset\partial T} h^2\big(|\mathbf{v}_t(\tilde{N}_{jk})|^2 + |\mathbf{v}_t(\tilde{N}_{kj})|^2\big) \;\lesssim\; \|\hat{\mathbf{v}}\|^2_{\mathbf{L}^2(T)}\,. \tag{5.29}$$

Let e_{jk} be one of the edges of T. Due to (5.26) and a scaling argument on the reference quadrilateral we see that

$$h\,\|\overline{v}_n\|^2_{L^2(e_{jk})} \;\simeq\; h\,\|\overline{v}_n\|^2_{L^2(\tilde{e}_{jk})} \;=\; h\,\|\hat{v}_n\|^2_{L^2(\tilde{e}_{jk})} \;\lesssim\; \|\hat{\mathbf{v}}\|^2_{\mathbf{L}^2(Q_{jk})}\,. \tag{5.30}$$

Summing estimate (5.29) over all elements and estimate (5.30) over all element edges of the mesh yields the desired result. ∎

LEMMA 5.12. *The operator $\mathcal{Y}^{(i)}$ is continuous with respect to the H^1 semi-norms:*

$$|\mathcal{Y}^{(i)}\hat{\mathbf{v}}^{(i)}|_{\mathbf{H}^1(\Omega^{(i)},\mathcal{T}_h^{(i)})} \;\lesssim\; |\hat{\mathbf{v}}^{(i)}|_{H^1(\Omega^{(i)})} \qquad \forall \hat{\mathbf{v}}^{(i)} \in \hat{\mathbf{V}}_h^{(i)}. \tag{5.31}$$

Proof. As in the proof of Lemma 5.8, all reference to the subdomain index (i) shall be omitted. Let $\hat{\mathbf{v}}^{(i)} \in \hat{\mathbf{V}}_h^{(i)}$ be an arbitrary but fixed continuous finite element function on the refined mesh $\mathcal{T}_h^{\mathrm{ref},(i)}$ and $(\mathbf{v}^{(i)}, \overline{v}_n^{(i)}) := \mathcal{Y}^{(i)}\hat{\mathbf{v}}^{(i)} \in \mathbf{V}_h^{(i)} \times \overline{V}_{n,h}^{(i)}$ its TDNNS counterpart. Furthermore, we define

$$\overline{\hat{\mathbf{v}}}^{\omega_T} := \frac{1}{|\omega_T|}\int_{\omega_T} \hat{\mathbf{v}}\,dx, \tag{5.32}$$

i.e., the average of $\hat{\mathbf{v}}$ on the element patch ω_T. By a standard inverse inequality, we obtain

$$|\mathcal{X}\mathcal{Y}\hat{\mathbf{v}}|^2_{\mathbf{H}^1(T)} \;=\; |\mathcal{X}\mathcal{Y}\hat{\mathbf{v}} - \overline{\hat{\mathbf{v}}}^{\omega_T}|^2_{\mathbf{H}^1(T)} \;\lesssim\; h^{-2}\|\mathcal{X}\mathcal{Y}\hat{\mathbf{v}} - \overline{\hat{\mathbf{v}}}^{\omega_T}\|^2_{\mathbf{L}^2(T)}\,. \tag{5.33}$$

Since the (global) operators $\mathcal{X}$ and $\mathcal{Y}$ preserve constant vector fields, and because of the L^2-estimates (5.23) and (5.27) from Lemma 5.9 and Lemma 5.11,

$$\|\mathcal{X}\mathcal{Y}\hat{\mathbf{v}} - \overline{\hat{\mathbf{v}}}^{\omega_T}\|^2_{\mathbf{L}^2(T)} \;=\; \|\mathcal{X}\mathcal{Y}(\hat{\mathbf{v}} - \overline{\hat{\mathbf{v}}}^{\omega_T})\|^2_{\mathbf{L}^2(T)} \;\lesssim\; \|\hat{\mathbf{v}} - \overline{\hat{\mathbf{v}}}^{\omega_T}\|^2_{\mathbf{L}^2(\omega_T)}\,. \tag{5.34}$$

A Poincaré inequality on ω_T yields

$$\|\hat{\mathbf{v}} - \overline{\hat{\mathbf{v}}}^{\omega_T}\|^2_{\mathbf{L}^2(\omega_T)} \;\lesssim\; h^2\,|\hat{\mathbf{v}}|^2_{\mathbf{H}^1(\omega_T)}. \tag{5.35}$$

The hidden constant depends only on the constant of shape regularity. Combining (5.33)–(5.35), summing over all $T \in \mathcal{T}_h$ and using that the patches ω_T have finite overlap, we get

$$|\mathcal{X}\mathcal{Y}\hat{\mathbf{v}}|_{\mathbf{H}^1(\Omega)} \;\lesssim\; |\hat{\mathbf{v}}|_{\mathbf{H}^1(\Omega)}. \tag{5.36}$$

An application of Lemma 5.8 helps to obtain the desired result

$$|\mathcal{Y}\hat{\mathbf{v}}|_{\mathbf{H}^1(\Omega,\mathcal{T}_h)} \simeq |\mathcal{X}\mathcal{Y}\hat{\mathbf{v}}|_{\mathbf{H}^1(\Omega)} \lesssim |\hat{\mathbf{v}}|_{\mathbf{H}^1(\Omega)}. \tag{5.37}$$

∎

5.3. A Cutoff Estimate. In this section, we provide a TDNNS counterpart to a known cutoff estimate for continuous FE functions. The following assumption is essentially [39, Assumption 4.3].

ASSUMPTION 5.13. *Each subdomain $\Omega^{(i)}$ is the union of a few elements from a shape-regular coarse triangulation of Ω.*

In the sequel, the subdomain diameter is denoted by $H^{(i)} := \operatorname{diam}(\Omega^{(i)})$. Note that the shape-regularity implies that the diameters of adjacent subdomains $\Omega^{(i)}$, $\Omega^{(j)}$ are comparable: $H^{(i)} \simeq H^{(j)}$.

LEMMA 5.14. *Let Assumption 5.13 hold and let $\mathcal{E}^{(ij)}$ be a subdomain edge of $\Omega^{(i)}$. Then for all $(\mathbf{v}^{(i)}, \overline{v}_n^{(i)}) \in \mathbf{V}_h^{(i)} \times \overline{V}_{n,h}^{(i)}$ there exists $(\mathbf{w}^{(i)}, \overline{w}_n^{(i)}) \in \mathbf{V}_h^{(i)} \times \overline{V}_{n,h}^{(i)}$ with*

$$\mathbf{w}_t^{(i)} = \begin{cases} \mathbf{v}_t^{(i)} & \text{on } \mathcal{E}^{(ij)} \\ 0 & \text{on } \partial\Omega^{(i)} \setminus \mathcal{E}^{(ij)} \end{cases} \qquad \overline{w}_n^{(i)} = \begin{cases} \overline{v}_n^{(i)} & \text{on } \mathcal{E}^{(ij)} \\ 0 & \text{on } \partial\Omega^{(i)} \setminus \mathcal{E}^{(ij)} \end{cases} \tag{5.38}$$

such that

$$|\mathbf{w}^{(i)}, \overline{w}_n^{(i)}|^2_{\mathbf{H}^1(\Omega^{(i)}, \mathcal{T}_h^{(i)})} \lesssim (1 + \log(\tfrac{H^{(i)}}{h}))^2 \, \|\mathbf{v}^{(i)}, \overline{v}_n^{(i)}\|^2_{\mathbf{H}^1(\Omega^{(i)}, \mathcal{T}_h^{(i)})}, \tag{5.39}$$

with the full norm from (3.16). *The hidden constant only depends on the shape of $\Omega^{(i)}$ and on the shape-regularity and quasi-uniformity constant of $\mathcal{T}_h^{(i)}$. Moreover, if $\mathbf{v}^{(i)} \in \mathbf{P}^1$ and $\overline{v}_n^{(i)}$ its normal component, then*

$$|\mathbf{w}^{(i)}, \overline{w}_n^{(i)}|^2_{\mathbf{H}^1(\Omega^{(i)}, \mathcal{T}_h^{(i)})} \lesssim (1 + \log(\tfrac{H^{(i)}}{h})) \, \|\mathbf{v}^{(i)}\|^2_{\mathbf{L}^\infty(\mathcal{E}^{(ij)})}. \tag{5.40}$$

If the mesh $\mathcal{T}_h^{(i)}$ is only shape regular, then (5.39), (5.40) *still hold if h in the logarithmic terms is replaced by the smallest diameter of the elements touching $\mathcal{E}^{(ij)}$.*

Proof. In this proof, we simply omit the superscripts (i) and (ij). For fixed $(\mathbf{v}, \overline{v}_n) \in \mathbf{V}_h \times \overline{V}_{n,h}$, we first set $\hat{\mathbf{v}} := \mathcal{X}(\mathbf{v}, \overline{v}_n)$. Thanks to the scalar inequality from [23, Lemma 4.4] (see also [5, Lemma 3.5], [29, Theorem 4.6] for earlier versions), it follows that there exists a function $\hat{\mathbf{w}} \in \hat{\mathbf{V}}$ such that

$$\begin{aligned} \hat{\mathbf{w}}(N) &= \hat{\mathbf{v}}(N) && \text{for interior nodes } N \text{ of } \mathcal{E} \text{ in } \mathcal{T}_h^{\mathrm{ref}}, \\ \hat{\mathbf{w}} &= 0 && \text{on } \partial\Omega \setminus \mathcal{E}, \end{aligned} \tag{5.41}$$

and

$$|\hat{\mathbf{w}}|^2_{\mathbf{H}^1(\Omega)} \lesssim (1 + \log(\tfrac{H}{h}))^2 \left(|\hat{\mathbf{v}}|^2_{\mathbf{H}^1(\Omega)} + H^{-2} \, \|\hat{\mathbf{v}}\|^2_{L^2(\Omega)} \right). \tag{5.42}$$

The hidden constant only depends on the shape-regularity constants of $\mathcal{T}_h$ and the coarse triangulation from Assumption 5.13. By setting $(\mathbf{w}, \overline{w}_n) := \mathcal{Y}\hat{\mathbf{w}}$, we obtain (5.39) immediately from Lemma 5.12, (5.42), Lemma 5.8, and Lemma 5.9.

If $\mathbf{v} \in \mathbf{P}^1$, then $\hat{\mathbf{v}} = \mathbf{v} \in \mathbf{P}^1$. In that case, $\hat{\mathbf{w}} \in \hat{\mathbf{V}}$ can be chosen such that (5.41) holds and

$$|\hat{\mathbf{w}}|^2_{\mathbf{H}^1(\Omega)} \lesssim (1 + \log(\tfrac{H}{h})) \, \|\hat{\mathbf{v}}\|^2_{L^\infty(\mathcal{E})}, \tag{5.43}$$

see [27, Lemma 7.1] and the references therein. Eventually, this implies (5.40). ∎

REMARK 5.15. *In view Lemma 5.14, Assumption 5.13 can be relaxed. In [23, Lem. 4.4], it was shown that* (5.42) *holds even if $\Omega^{(i)}$ is a only a John domain. In that case, the hidden constant depends on the John parameter of $\Omega^{(i)}$ (cf. [23, Def. 2.1]) and on the shape-regularity constant of $\mathcal{T}_h^{(i)}$. This helps to provide some theory for subdomain decompositions are generated by graph partitioning (e.g. METIS) that lead to irregular interfaces, cf. [23, Thm. 4.1].*

5.4. A Subdomain Transfer Operator. The next lemma provides a TDNNS counterpart to an extension operator for continuous FE functions, cf. [35, Sect. 2.5.7].

LEMMA 5.16. *Let Assumption 5.13 hold and let $\Omega^{(i)}$, $\Omega^{(j)}$ be subdomains that share the subdomain edge $\mathcal{E}^{(ij)}$. Then there exists an extension operator*

$$\mathbb{E}^{(i\to j)} : \mathbf{V}_h^{(i)} \times \overline{V}_{n,h}^{(i)} \to \mathbf{V}_h^{(j)} \times \overline{V}_{n,h}^{(j)} : (\mathbf{v}, \overline{v}_n) \mapsto (\mathbf{w}, \overline{w}_n) \tag{5.44}$$

such that

$$\mathbf{w}_t = \mathbf{v}_t,\ \overline{w}_n = \overline{v}_n \ \text{ on } \mathcal{E}^{(ij)} \tag{5.45}$$

$$\|\mathbf{w}\|^2_{L^2(\Omega^{(j)})} + \sum_{T\in\mathcal{T}_h^{(j)}} h\|\overline{w}_n\|^2_{L^2(\partial T)} \ \lesssim\ \|\mathbf{v}\|^2_{L^2(\Omega^{(i)})} + \sum_{T\in\mathcal{T}_h^{(i)}} h\|\overline{v}_n\|^2_{L^2(\partial T)} \tag{5.46}$$

$$|\mathbf{w}, \overline{w}_n|^2_{\mathbf{H}^1(\Omega^{(j)},\mathcal{T}_h^{(j)})} \ \lesssim\ |\mathbf{v}, \overline{v}_n|^2_{\mathbf{H}^1(\Omega^{(i)},\mathcal{T}_h^{(i)})}\,. \tag{5.47}$$

The hidden constants only depend on the shape-regularity constant of the coarse mesh from Assumption 5.13 and on the shape-regularity constant of $\mathcal{T}_h(\Omega)$. In particular,

$$\|\mathbb{E}^{(i\to j)}(\mathbf{v}, \overline{v}_n)\|_{\mathbf{H}^1(\Omega^{(j)},\mathcal{T}_h^{(j)})} \ \lesssim\ \|\mathbf{v}, \overline{v}_n\|_{\mathbf{H}^1(\Omega^{(i)},\mathcal{T}_h^{(i)})}\,. \tag{5.48}$$

Proof. Let $\widehat{\mathbb{E}}^{(i\to j)} : \hat{\mathbf{V}}_h^{(i)} \to \hat{\mathbf{V}}_h^{(j)}$ be a discrete extension operator such that

$$\begin{aligned} \widehat{\mathbb{E}}^{(i\to j)}\hat{\mathbf{v}} \ &=\ \hat{\mathbf{v}} \text{ on } \mathcal{E}^{(ij)}, \\ \|\mathbb{E}^{(i\to j)}\hat{\mathbf{v}}\|_{\mathbf{L}^2(\Omega^{(j)})} \ &\lesssim\ \|\mathbb{E}^{(i\to j)}\hat{\mathbf{v}}\|_{\mathbf{L}^2(\Omega^{(i)})}\,, \\ |\mathbb{E}^{(i\to j)}\hat{\mathbf{v}}|_{\mathbf{H}^1(\Omega^{(j)})} \ &\lesssim\ |\mathbb{E}^{(i\to j)}\hat{\mathbf{v}}|_{\mathbf{H}^1(\Omega^{(i)})} \end{aligned} \tag{5.49}$$

for all $\hat{\mathbf{v}} \in \hat{\mathbf{V}}_h^{(i)}$). For an explicit construction in the scalar case see, e.g., [35, Sect. 2.5.7]. The vectorial case is then straightforward. By setting

$$\mathbb{E}^{(i\to j)} := \mathcal{Y}^{(j)}\, \widehat{\mathbb{E}}^{(i\to j)}\, \mathcal{X}^{(i)}$$

the properties stated in the lemma follow from (5.49), Lemma 5.8, Lemma 5.9, Lemma 5.11, and Lemma 5.12. ∎

REMARK 5.17. *The results of Lemma 5.16, except for* (5.48)*, also hold under the much milder assumptions that $\Omega^{(i)}$, $\Omega^{(j)}$ are Jones domains (uniform domains). In such a case, the proof works the same line using an adaption of Jones' extension operator [22], and the hidden constants then depend only on the respective Jones parameters. See [23, Lemma 4.5] for a similar application to FETI-DP.*

5.5. Proof of Estimate (5.4)**.** For the sake of simplicity, we present the proofs in this section only for variant (a). The proofs for variant (b) can be obtained analogously. Recall that for simplicity, we have assumed from the beginning that $\mathcal{T}_h$ is globally quasi-uniform. For the results below, however, we only need that the *local* subdomain meshes $\mathcal{T}_h^{(i)}$ are quasi-uniform with mesh parameter $h^{(i)}$. Therefore, to formulate our estimates, we use the notation

$$H/h := \max_{i=1,\dots,N} \frac{H^{(i)}}{h^{(i)}},$$

which is rather common in the literature on iterative substructuring methods, cf. [39, Sect. 4.2]. For extensions to more general meshes see also Sect. 5.7 below.

LEMMA 5.18. *Let Assumption 5.13 hold. Then*

$$|\underline{\mathbf{P}}_D\mathbf{W}|_{\underline{\mathbf{S}}}^2 \;\le\; C\,(1+\log(H/h))^2\,|\mathbf{W}|_{\underline{\mathbf{S}}}^2 \qquad \forall \mathbf{W}\in\mathbb{W}^\perp.$$

The constant C depends on the shape-regularity and quasi-uniformity constants of $\mathcal{T}_h^{(i)}$ and the coarse mesh from Assumption 5.13 as well as on the Poisson ratio ν. However, C is independent of h, $H^{(i)}$, the Young moduli $E^{(i)}$, and the number of subdomains.

Proof. Beforehand, we collect a few facts on the involved (semi)norms and the Schur complement $\underline{\mathbf{S}}^{(i)}$ of $\underline{\mathbf{K}}^{(i)}$. From the definition of $\mathbb{W}^{(i)}$ (Def. 5.2), we get

$$|\mathbf{U}|_{\underline{\mathbf{S}}^{(i)}} = |\mathbf{U}|_{\underline{\mathbf{K}}^{(i)}} \quad \forall \mathbf{U}\in\mathbb{W}^{(i)}. \tag{5.50}$$

Employing standard estimates, we find that

$$|\mathbf{U}|_{\underline{\mathbf{S}}^{(i)}}^2 \lesssim E^{(i)}\,|(\mathbf{u},\overline{u}_n)|_{\mathbf{H}^1(\Omega^{(i)},\mathcal{T}_h^{(i)})}^2 \quad \forall \mathbf{U}\leftrightarrow(\mathbf{u},\overline{u}_n)\in\mathbf{V}_h^{(i)}\times\overline{V}_{n,h}^{(i)}\,, \tag{5.51}$$

where the hidden constant only depends on ν. From the Korn inequality in [7] and the Poincaré/Friedrichs inequality in [6] (see also [33]), one can conclude that

$$|\mathbf{U}|_{\underline{\mathbf{K}}^{(i)}}^2 \gtrsim E^{(i)}\,\|(\mathbf{u},\overline{u}_n)\|_{\mathbf{H}^1(\Omega^{(i)},\mathcal{T}_h^{(i)})}^2 \quad \text{for } \mathbf{U}\leftrightarrow(\mathbf{u},\overline{u}_n),\ \int_{\Omega^{(i)}}\mathbf{u}\cdot\mathbf{z}\,dx=0\ \ \forall \mathbf{z}\in\mathcal{RB}, \tag{5.52}$$

where the hidden constants depend on Poisson's ratio ν, the classical Korn and Poincaré constant of $\Omega^{(i)}$, and on the shape-regularity constant of $\mathcal{T}_h^{(i)}$. The same estimate holds if $\partial\Omega^{(i)}\cap\Gamma_D$ has positive surface measure and if the orthogonality condition in (5.52) is replaced by the boundary condition $\mathbf{u}|_{\Gamma_D}=0$.

We now begin with the actual proof. Let $\mathbf{W}\in\mathbb{W}^\perp$ be arbitrary but fixed and let $(\mathbf{w}^{(i)},\overline{w}_n^{(i)})\in\mathcal{W}^{(i),\perp}$ denote the corresponding local functions. Recall formula (5.2) (for variant (a)),

$$(\underline{\mathbf{P}}_D\mathbf{W})_k^{(i)} \;=\; \begin{cases}\delta_{\dagger,\mathcal{E}^{(ij)}}^{(j)}\big(W_k^{(i)}-W_\ell^{(j)}\big) & \text{if } (i,k)\sim(j,\ell) \text{ on } \mathcal{E}^{(ij)},\\ 0 & \text{else.}\end{cases} \tag{5.53}$$

Let $\underline{\Xi}_{\mathcal{E}^{(ij)}}$ be the (generic) matrix that sets to zero all the dofs that are not associated to the subdomain edge $\mathcal{E}^{(ij)}$. From formula (5.53), the triangle inequality, and the fact that the number of subdomain edges per subdomain is uniformly bounded, we obtain with a slight abuse of notation that

$$\begin{aligned}|(\underline{\mathbf{P}}_D\mathbf{W})^{(i)}|_{\underline{\mathbf{S}}^{(i)}}^2 &\lesssim \sum_{j:\mathcal{E}^{(ij)}\neq\emptyset}|\underline{\Xi}_{\mathcal{E}^{(ij)}}(\underline{\mathbf{P}}_D\mathbf{W})^{(i)}|_{\underline{\mathbf{S}}^{(i)}}^2\\ &= \sum_{j:\mathcal{E}^{(ij)}\neq\emptyset}(\delta_{\dagger,\mathcal{E}^{(ij)}}^{(j)})^2\,|\underline{\Xi}_{\mathcal{E}^{(ij)}}(\mathbf{W}^{(i)}-\mathbf{W}^{(j)})|_{\underline{\mathbf{S}}^{(i)}}^2\\ &\lesssim \sum_{j:\mathcal{E}^{(ij)}\neq\emptyset}\Big(|\underline{\Xi}_{\mathcal{E}^{(ij)}}\mathbf{W}^{(i)}|_{\underline{\mathbf{S}}^{(i)}}^2+\frac{E^{(j)}}{E^{(i)}}\,|\underline{\Xi}_{\mathcal{E}^{(ij)}}\mathbf{W}^{(j)}|_{\underline{\mathbf{S}}^{(i)}}^2\Big),\end{aligned} \tag{5.54}$$

where in the last step we have used the elementary inequality (4.10).

For the first term on the right-hand side, (5.51) and Lemma 5.14 yield

$$|\underline{\Xi}_{\mathcal{E}^{(ij)}}\mathbf{W}^{(i)}|_{\underline{\mathbf{S}}^{(i)}}^2 \;\lesssim\; (1+\log(\tfrac{H^{(i)}}{h}))^2\,E^{(i)}\,\|\mathbf{w}^{(i)},\overline{w}_n^{(i)}\|_{\mathbf{H}^1(\Omega^{(i)},\mathcal{T}_h^{(i)})}^2\,. \tag{5.55}$$

From the properties of the transfer operator $\mathbb{E}^{(j\to i)}$ (Lemma 5.16), we see that the corresponding dofs of the functions $(\mathbf{w}^{(j)}, \overline{w}_n^{(j)})$ and $\mathbb{E}^{(j\to i)}(\mathbf{w}^{(j)}, \overline{w}_n^{(j)})$ coincide on $\mathcal{E}^{(ij)}$. Hence, (5.51), Lemma 5.14, and estimate (5.48) imply

$$
\begin{aligned}
|\Xi_{\mathcal{E}^{(ij)}}\mathbf{W}^{(j)}|^2_{\underline{\mathbf{S}}^{(i)}} &\le (1+\log(\tfrac{H^{(i)}}{h}))^2\, E^{(i)}\, \|\mathbb{E}^{(j\to i)}(\mathbf{w}^{(j)}, \overline{w}_n^{(j)})\|^2_{\mathbf{H}^1(\Omega^{(i)},\mathcal{T}_h^{(i)})} \\
&\le (1+\log(\tfrac{H^{(i)}}{h}))^2\, E^{(i)}\, \|\mathbf{w}^{(j)}, \overline{w}_n^{(j)}\|^2_{\mathbf{H}^1(\Omega^{(j)},\mathcal{T}_h^{(j)})}\,.
\end{aligned} \tag{5.56}
$$

Combining (5.54)–(5.56), we get

$$
\begin{aligned}
|(\underline{\mathbf{P}}_D\mathbf{W})^{(i)}|^2_{\underline{\mathbf{S}}^{(i)}} \lesssim \sum_{j:\mathcal{E}^{(ij)}\neq\emptyset} (1+\log(\tfrac{H^{(i)}}{h}))^2 \Big(& E^{(i)}\, \|\mathbf{w}^{(i)}, \overline{w}_n^{(i)}\|^2_{\mathbf{H}^1(\Omega^{(i)},\mathcal{T}_h^{(i)})} \\
& + E^{(j)}\, \|\mathbf{w}^{(j)}, \overline{w}_n^{(j)}\|^2_{\mathbf{H}^1(\Omega^{(j)},\mathcal{T}_h^{(j)})}\Big).
\end{aligned} \tag{5.57}
$$

Recall that $\mathbf{W}\in\mathbb{W}^\perp$, and so the corresponding local functions either vanish on the Dirichlet boundary, or they are orthogonal to $\mathcal{RB}$. Hence, due to estimate (5.52),

$$
|(\underline{\mathbf{P}}_D\mathbf{W})^{(i)}|^2_{\underline{\mathbf{S}}^{(i)}} \lesssim \sum_{j:\mathcal{E}^{(ij)}\neq\emptyset} (1+\log(\tfrac{H^{(i)}}{h}))^2 \Big(|\mathbf{W}^{(i)}|^2_{\underline{\mathbf{K}}^{(i)}} + |\mathbf{W}^{(j)}|^2_{\underline{\mathbf{K}}^{(j)}} \Big). \tag{5.58}
$$

Because of (5.50), the $\underline{\mathbf{K}}$-norms above can be replaced by the $\underline{\mathbf{S}}$-norms. The final estimate now follows immediately by summing (5.58) over $i=1,\dots,N$ and using that the number of subdomain edges per subdomain is uniformly bounded. ∎

REMARK 5.19. *As seen from the above proof and from Remarks 5.15 and 5.17, Assumption 5.13 is not essential for Lemma 5.18.*

The next lemma provides a bound for $\underline{\mathbf{P}}_D\mathbf{Z}_\mathbf{W}$.

LEMMA 5.20. *Let Assumption 5.13 hold. Then for* $\underline{\mathbf{Q}} = \underline{\mathbf{Q}}_{\mathrm{diag}}$,

$$
|\underline{\mathbf{P}}_D\mathbf{Z}_\mathbf{W}|^2_{\underline{\mathbf{S}}} \le C\,(1+\log(H/h))\,|\mathbf{W}|^2_{\underline{\mathbf{S}}} \qquad \forall \mathbf{W}\in\mathbb{W}^\perp,
$$

with a constant C as in Lemma 5.18.

Proof. For simplicity, let $\mathbf{Z}^{(i)}$ denote the components of $\mathbf{Z}_\mathbf{W}$. Recall that each local function $\mathbf{Z}^{(i)}\in\mathcal{RB}$ is continuous on $\Omega^{(i)}$. Applying estimate (5.54) from the proof of Lemma 5.18 (with $\mathbf{W}\mapsto\mathbf{Z}_\mathbf{W}$), we get

$$
|(\underline{\mathbf{P}}_D\mathbf{Z}_\mathbf{W})^{(i)}|^2_{\underline{\mathbf{S}}^{(i)}} \lesssim \sum_{j:\mathcal{E}^{(ij)}\neq\emptyset} (\delta^{(i)}_{\dagger,\mathcal{E}^{(ij)}})^2\, (|\Xi_{\mathcal{E}^{(ij)}}(\mathbf{Z}^{(i)}-\mathbf{Z}^{(j)})|^2_{\underline{\mathbf{S}}^{(i)}}\,, \tag{5.59}
$$

where the (restriction) matrix $\Xi_{\mathcal{E}^{(ij)}}$ sets to zero all dofs not associated to $\mathcal{E}^{(ij)}$. For $(\mathbf{z}^{(i)}, \overline{z}_n^{(i)}) \leftrightarrow \mathbf{Z}^{(i)}$, we obtain from (5.51), (4.10), and Lemma 5.14 that

$$
(\delta^{(i)}_{\dagger,\mathcal{E}^{(ij)}})^2\, |\Xi_{\mathcal{E}^{(ij)}}(\mathbf{Z}^{(i)}-\mathbf{Z}^{(j)})|^2_{\underline{\mathbf{S}}^{(i)}} \le (1+\log(\tfrac{H^{(i)}}{h}))\min(E^{(i)},E^{(j)})\|\mathbf{z}^{(i)}-\mathbf{z}^{(j)}\|^2_{\mathbf{L}^\infty(\mathcal{E}^{(ij)})}, \tag{5.60}
$$

where we have used that $\mathbf{z}^{(i)}$, $\mathbf{z}^{(j)}\in\mathcal{RB}\subset\mathbf{P}^1$ and $\overline{z}_n^{(i)}$, $\overline{z}_n^{(j)}$ are the corresponding normal components. Using Assumption 5.13 and the quasi-uniformity of $\mathcal{T}_h^{(i)}$ (alternatively Assumption 5.23 below), one can easily show from the definition of the Nédélec dofs (3.19) that

$$
\|\mathbf{z}^{(i)}-\mathbf{z}^{(j)}\|^2_{\mathbf{L}^\infty(\mathcal{E}^{(ij)})} \simeq \frac{1}{H^{(ij)}}\|\mathbf{z}^{(i)}-\mathbf{z}^{(j)}\|^2_{\mathbf{L}^2(\mathcal{E}^{(ij)})} \lesssim \frac{1}{h\,H^{(ij)}}\|\Xi_{\mathcal{E}^{(ij)}}(\mathbf{Z}^{(i)}-\mathbf{Z}^{(j)})\|^2_{\ell^2}\,, \tag{5.61}
$$

where $\|\cdot\|_{\ell^2}$ denotes the Euclidean vector norm. The entries of $\Xi_{\mathcal{E}^{(ij)}}(\mathbf{Z}^{(i)} - \mathbf{Z}^{(j)})$ are exactly the entries of $\underline{\mathbf{B}}\mathbf{Z}_{\mathbf{W}}$ associated to coupling dofs on $\mathcal{E}^{(ij)}$. Using this fact, combining (5.59)–(5.61), summing over $i = 1, \dots, N$ and pulling out the maximum of the logarithmic factors yields

$$|\underline{\mathbf{P}}_D \mathbf{Z}_{\mathbf{W}}|^2_{\underline{\mathbf{S}}} \lesssim (1 + \log(H/h)) \sum_{\mathcal{E}^{(ij)} \neq \emptyset} \frac{\min(E^{(i)}, E^{(j)})}{h\, H^{(ij)}} \|(\underline{\mathbf{B}}\mathbf{Z}_{\mathbf{W}})|_{\mathcal{E}^{(ij)}}\|^2_{\ell^2}\,. \tag{5.62}$$

Combining the latter with the definition (4.14) of $\underline{\mathbf{Q}}_{\mathrm{diag}}$ and with Lemma 5.3 yields

$$|\underline{\mathbf{P}}_D \mathbf{Z}_{\mathbf{W}}|^2_{\underline{\mathbf{S}}} \lesssim \|\underline{\mathbf{B}}\mathbf{Z}_{\mathbf{W}}\|^2_{\underline{\mathbf{Q}}_{\mathrm{diag}}} \lesssim \|\underline{\mathbf{B}}\mathbf{W}\|^2_{\underline{\mathbf{Q}}_{\mathrm{diag}}}\,. \tag{5.63}$$

From the definition of $\underline{\mathbf{Q}}_{\mathrm{diag}}$ and the triangle inequality, we conclude that

$$\|\underline{\mathbf{B}}\mathbf{W}\|^2_{\underline{\mathbf{Q}}_{\mathrm{diag}}} \simeq \sum_{\mathcal{E}^{(ij)} \neq \emptyset} \frac{\min(E^{(i)}, E^{(j)})}{h\, H^{(ij)}} \|\Xi_{\mathcal{E}^{(ij)}}(\mathbf{W}^{(i)} - \mathbf{W}^{(j)})\|^2_{\ell^2} \tag{5.64}$$

$$\lesssim \sum_{\mathcal{E}^{(ij)} \neq \emptyset} \frac{1}{H^{(ij)}} \Big(\frac{E^{(i)}}{h} \|\Xi_{\mathcal{E}^{(ij)}} \mathbf{W}^{(i)}\|^2_{\ell^2} + \frac{E^{(j)}}{h} \|\Xi_{\mathcal{E}^{(ij)}} \mathbf{W}^{(j)}\|^2_{\ell^2} \Big). \tag{5.65}$$

Due to the choice of the dofs and due to quasi-uniformity (or Assumption 5.23 below), we have

$$h^{-1} \|\Xi_{\mathcal{E}^{(ij)}} \mathbf{W}^{(i)}\|^2_{\ell^2} \simeq \|\mathbf{w}_t^{(i)}\|^2_{\mathbf{L}^2(\mathcal{E}^{(ij)})} + \|\overline{w}_n^{(i)}\|^2_{L^2(\mathcal{E}^{(ij)})}. \tag{5.66}$$

From the construction of $\mathcal{X}$, one sees that for $\hat{\mathbf{w}} = \mathcal{X}(\mathbf{w}^{(i)}, \overline{w}_n^{(i)})$,

$$\|\mathbf{w}_t^{(i)}\|^2_{\mathbf{L}^2(\mathcal{E}^{(ij)})} + \|\overline{w}_n^{(i)}\|^2_{L^2(\mathcal{E}^{(ij)})} \lesssim \|\hat{\mathbf{w}}^{(i)}\|^2_{\mathbf{L}^2(\mathcal{E}^{(ij)})}\,. \tag{5.67}$$

A standard trace theorem in H^1 combined with the stability estimates from Lemma 5.8 and Lemma 5.9 yields

$$\begin{aligned} \|\hat{\mathbf{w}}^{(i)}\|^2_{\mathbf{L}^2(\mathcal{E}^{(ij)})} &\lesssim H^{(i)}\, |\hat{\mathbf{w}}^{(i)}|^2_{\mathbf{H}^1(\Omega^{(i)})} + \frac{1}{H^{(i)}}\, \|\hat{\mathbf{w}}^{(i)}\|^2_{\mathbf{L}^2(\Omega^{(i)})} \\ &\lesssim H^{(i)}\, \|\mathbf{w}^{(i)}, \overline{w}_n^{(i)}\|^2_{\mathbf{H}^1(\Omega^{(i)}, \mathcal{T}_h^{(i)})}\,, \end{aligned} \tag{5.68}$$

where the hidden constant only depends on the shape of $\Omega^{(i)}$ and the shape-regularity of $\mathcal{T}_h^{(i)}$. Combining (5.62)–(5.68), we obtain

$$\begin{aligned} |\underline{\mathbf{P}}_D \mathbf{Z}_{\mathbf{W}}|^2_{\underline{\mathbf{S}}} \lesssim (1 + \log(\tfrac{H}{h})) \sum_{\mathcal{E}^{(ij)} \neq \emptyset} \frac{H^{(i)}}{H^{(ij)}} \Big(& E^{(i)}\, \|\mathbf{w}^{(i)}, \overline{w}_n^{(i)}\|^2_{\mathbf{H}^1(\Omega^{(i)}, \mathcal{T}_h^{(i)})} \\ & + E^{(j)}\, \|\mathbf{w}^{(j)}, \overline{w}_n^{(j)}\|^2_{\mathbf{H}^1(\Omega^{(j)}, \mathcal{T}_h^{(j)})} \Big). \end{aligned} \tag{5.69}$$

Thanks to Assumption 5.13, $H^{(i)}/H^{(ij)} \simeq 1$. Due to (5.52) and (5.50), it follows that

$$|\underline{\mathbf{P}}_D \mathbf{Z}_{\mathbf{W}}|^2_{\underline{\mathbf{S}}} \lesssim (1 + \log(\tfrac{H}{h})) \sum_{\mathcal{E}^{(ij)} \neq \emptyset} \Big(|\mathbf{W}^{(i)}|^2_{\underline{\mathbf{S}}^{(i)}} + |\mathbf{W}^{(j)}|^2_{\underline{\mathbf{S}}^{(i)}} \Big). \tag{5.70}$$

Using that the number of subdomain edges per subdomain is uniformly bounded, one can easily conclude the proof. ∎

5.6. Condition Number Estimate. THEOREM 5.21. *Let* $\underline{\mathbf{Q}} = \underline{\mathbf{Q}}_{\mathrm{diag}}$ *and let Assumption 5.13 hold. Then*

$$\kappa(\underline{\mathbf{P}}\,\underline{\mathbf{M}}^{-1}\underline{\mathbf{P}}^{\top}\underline{\mathbf{F}}_{|\boldsymbol{\Lambda}_{\mathrm{ad}}}) \;\leq\; C\,(1+\log(H/h))^2.$$

The constant C depends on the shape-regularity and quasi-uniformity constants of $\mathcal{T}_h^{(i)}$ and the coarse mesh from Assumption 5.13 as well as on the Poisson ratio ν. However, C is independent of h, $H^{(i)}$, the Young moduli $E^{(i)}$, and the number of subdomains.

Proof. Follows from Lemma 5.4, Lemma 5.18, and Lemma 5.20. ∎

REMARK 5.22. *Provided that $\underline{\mathbf{M}}^{-1}$ is definite on* range($\underline{\mathbf{G}}$)*, one can easily show (following [39, Lem. 6.14]) that for $\underline{\mathbf{Q}} = \underline{\mathbf{M}}^{-1}$, the same condition number estimate holds as in Theorem 5.21. In that case, Assumption 5.13 can even be be relaxed, cf. Remark 5.19.*

5.7. Extensions to More General Meshes. The local quasi-uniformity assumption on $\mathcal{T}_h^{(i)}$ in all the results above can be dropped, however with the following restrictions.

1. The global mesh must be shape regular.
2. The fraction H/h appearing in the estimates must be replaced by

$$\max_{\mathcal{E}^{(ij)}} \frac{H^{(ij)}}{h_{\min}^{(ij)}}\,,$$

   where $h_{\min}^{(ij)}$ denotes the minimum mesh size on $\mathcal{E}^{(ij)}$. In variant (b), also the non-trivial Dirichlet edges $\partial\Omega^{(i)} \cap \Gamma_D$ have to be included in the above maximum, with the local fraction $H^{(iD)}/h_{\min}^{(iD)}$.
3. If $\underline{\mathbf{Q}} = \underline{\mathbf{Q}}_{\mathrm{diag}}$ is used, then Assumption 5.13 and (in addition) Assumption 5.23 below must be fulfilled; otherwise the proof of Lemma 5.20 cannot be generalized (at least not straightforwardly).

ASSUMPTION 5.23. *The restriction of the mesh $\mathcal{T}_h$ to each subdomain edge $\mathcal{E}^{(ij)}$ is quasi-uniform with mesh size $h^{(ij)}$. In variant (b), additionally the restriction of $\mathcal{T}_h$ to $\partial\Omega^{(i)} \cap \Gamma_D$ is quasi-uniform with mesh size $h^{(iD)}$.*

Summarizing, if local quasi-uniformity and Assumption 5.13 are dropped simultaneously, then for $\underline{\mathbf{Q}} = \underline{\mathbf{M}}^{-1}$, one can still prove Theorem 5.21, whereas for $\underline{\mathbf{Q}} = \underline{\mathbf{Q}}_{\mathrm{diag}}$ additional assumptions are likely to be needed.

6. Numerical Results. The FETI-TDNNS method has been implemented in the framework of the research software PARMAX (see `http://www.numa.uni-linz.ac.at/P19255/software`). For the factorization of the coarse matrix $\underline{\mathbf{G}}^{\top}\underline{\mathbf{Q}}\underline{\mathbf{G}}$ and of the interior blocks of the subdomain stiffness matrices, we use the direct solver PARDISO (see e.g. [37]). In Algorithm 1, the (subdomain-wise) application of the generalized inverse $(\underline{\mathbf{K}}^{(i)})^{\dagger}$ of the possibly singular subdomain stiffness matrix $\underline{\mathbf{K}}^{(i)}$ is necessary. A viable approach to realize $\mathbf{V} = (\underline{\mathbf{K}}^{(i)})^{\dagger}\mathbf{G}$, which is pursued in the current implementation, is to solve the saddle point system

$$\begin{bmatrix} \underline{\mathbf{K}}^{(i)} & \underline{\mathbf{C}}^{(i)} \\ (\underline{\mathbf{C}}^{(i)})^{\top} & 0 \end{bmatrix} \begin{bmatrix} \mathbf{V} \\ \boldsymbol{\mu} \end{bmatrix} = \begin{bmatrix} \mathbf{G} \\ 0 \end{bmatrix}.$$

The width of $\underline{\mathbf{C}}^{(i)}$ is of the dimension of the kernel of $\underline{\mathbf{K}}^{(i)}$. Different choices of $\underline{\mathbf{C}}^{(i)}$ are possible, e.g. setting either $\underline{\mathbf{C}}^{(i)} = \underline{\mathbf{R}}^{(i)}$ or $\underline{\mathbf{C}}^{(i)} = \underline{\mathbf{M}}^{(i)}\underline{\mathbf{R}}^{(i)}$ with $\underline{\mathbf{R}}^{(i)}$ from

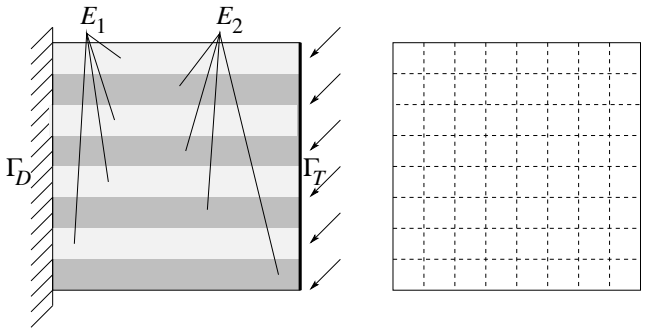

FIG. 6.1. *Sketch of problem setup.* Left: *Displacement and traction conditions, distribution of E-modulus in Sect. 6.2.* Right: *Subdomain decomposition.*

equation (4.2) and mass matrix $\underline{\mathbf{M}}^{(i)}$. Such saddle point systems can be efficiently solved by PARDISO as well.

In all the three following examples, we consider the plane strain model. The computational domain is a block of 8×8 mm, that is rigidly fixed at the left. A surface load and tractions are applied at the right edge Γ_T,

$$\mathbf{f}_V = 0, \qquad \mathbf{t}_{N|\Gamma_T} = (-125,\, -125)^\top \text{ N/mm}.$$

The latter corresponds to a total force of $\sqrt{2} \cdot 10^3$ N over the edge. The geometric setup and the subdomain decomposition into 8×8 square-shaped subdomains are shown in Figure 6.1.

The triangulation is a simple structured simplicial grid resolving the subdomain interfaces. In the computations we vary the resolution from $H/h = 2$ up to 32 edges in x- and y-direction per subdomain. This results in a global problem size of 3200 up to 788480 dofs (including Dirichlet dofs) for the reduced hybridized system.

In Tables 6.1–6.3, we display the condition numbers of the previously described (T)FETI method (variants (a) and (b)), estimated by the Lanczos method (column *cond*). Furthermore, we give the number of iterations of CG (column *iter*) needed to reduce the residual by a factor of 10^{-8}. The columns marked *CPU* contain the CPU time in seconds in sequential mode (neither using parallelization nor multithreading), needed for the total solve procedure. Here, the time for assembling the "Neumann" subdomain stiffness matrices was *excluded*, since these matrices are considered to be part of the *problem*, not the *solve*. All other assemblies and factorizations have been included. The computations were performed on a hp Z400 workstation with Intel Xeon Processor W3680 (3.33 GHz).

6.1. Compressible Case, Homogeneous Material. In our first example, we consider a homogeneous material distribution, $E = 2 \cdot 10^5$ N/mm^2, $\nu = 0.3$. Table 6.1 displays the results for FETI (variant (a)) and TFETI (variant (b)) with multiplicity scaling and with $\underline{\mathbf{Q}} = \underline{\mathbf{I}}$. The estimated condition numbers clearly confirm the estimate of Theorem 5.21. Note that we have 168 coarse dofs for FETI vs. 192 coarse dofs for TFETI. This explains why the condition numbers of TFETI are lower (because of a better coarse space). Note that the CPU time does not depend on conditioning alone, but also on the size of the coarse space.

6.2. Compressible Case, Heterogeneous Material. In our second example, we consider a heterogeneous material distribution with 8 horizontal layers of thickness

TABLE 6.1
Results for Sect. 6.1, multiplicity scaling, $\underline{\mathbf{Q}} = \underline{\mathbf{I}}$.

	FETI			TFETI		
H/h	cond	iter	CPU	cond	iter	CPU
2	15.37	22	0.34	3.24	15	0.31
4	19.82	28	1.17	5.34	20	1.04
8	25.00	34	4.86	8.43	25	4.39
16	30.03	38	25.73	11.84	29	24.45
32	35.19	42	193.93	15.59	33	201.02

TABLE 6.2
Results for Sect. 6.2.

		FETI			TFETI		
parameters	H/h	cond	iter	CPU	cond	iter	CPU
	2	$1.33 \cdot 10^5$	383	2.31	$2.85 \cdot 10^4$	338	2.53
multiplicity	4	$1.64 \cdot 10^5$	492	9.66	$3.58 \cdot 10^4$	467	10.04
scaling	8	$1.89 \cdot 10^5$	587	40.30	$4.97 \cdot 10^4$	559	41.72
$\underline{\mathbf{Q}} = \underline{\mathbf{I}}$	16	$2.15 \cdot 10^5$	684	184.74	$6.59 \cdot 10^4$	637	194.08
	32	$2.44 \cdot 10^5$	770	970.70	$8.42 \cdot 10^4$	716	1002.46
	2	2.76	12	0.41	3.54	15	0.46
coefficient	4	4.68	16	1.44	4.72	19	1.61
scaling	8	7.03	20	6.21	7.14	24	6.79
$\underline{\mathbf{Q}} = \underline{\mathbf{M}}^{-1}$	16	9.71	22	30.76	9.94	27	35.00
	32	12.71	24	218.40	13.12	30	250.62
	2	16.87	20	0.34	3.37	15	0.31
coefficient	4	22.09	24	1.10	4.96	19	1.02
scaling	8	27.73	29	4.55	8.45	24	4.47
$\underline{\mathbf{Q}} = \underline{\mathbf{Q}}_{\text{diag}}$	16	33.34	31	23.76	12.75	29	24.47
	32	39.09	35	186.27	17.82	32	200.08
	2	27.42	22	0.35	4.00	17	0.33
stiffness	4	34.85	26	1.13	5.33	20	1.04
scaling	8	42.85	30	4.73	8.45	24	4.38
$\underline{\mathbf{Q}} = \underline{\mathbf{Q}}_{\text{diag}}$	16	50.66	33	24.48	12.76	29	24.39
	32	58.54	36	187.38	17.83	32	200.36

1 mm, cf. Figure 6.1, left. Young's modulus alternates between $E_1 = 10$ N/mm^2 and $E_2 = 2 \cdot 10^5$ N/mm^2. Poisson's ratio is kept constant at $\nu = 0.3$. Obviously, the subdomain decomposition resolves the coefficient jumps, cf. Figure 6.1.

Table 6.2 summarizes the results. Again, both FETI and TFETI have been studied, but here with four different ways of choosing the scaling and $\underline{\mathbf{Q}}$ (see first column). The first choice (multiplicity scaling, $\underline{\mathbf{Q}} = \underline{\mathbf{I}}$) does not perform robustly: the condition number suffers from the large contrast of $2 \cdot 10^4$ in Young's modulus (see also the paragraph below). The other three choices are all robust with respect to the jumps, as our theory predicts. The best result concerning the conditioning is the coefficient scaling with $\underline{\mathbf{Q}} = \underline{\mathbf{M}}^{-1}$ (second block from top). However, for $\underline{\mathbf{Q}} = \underline{\mathbf{Q}}_{\text{diag}}$, the coarse matrix is much sparser, which results in shorter runtime for the two remaining choices. In this particular example, where the interfaces are straight edges, we see that coefficient and stiffness scaling lead to similar results.

Furthermore, we verify robustness for increasing contrast. Figure 6.2 shows the estimated condition numbers and the "solve" CPU times for the same setup with fixed discretization of $H/h = 16$, with E_1 fixed and with E_2/E_1 varying between 10^0 and 10^7. For the multiplicity scaling with $\underline{\mathbf{Q}} = \underline{\mathbf{I}}$, the condition numbers and CPU times blow up, whereas they stay almost constant for the stiffness scaling with $\underline{\mathbf{Q}} = \underline{\mathbf{Q}}_{\text{diag}}$.

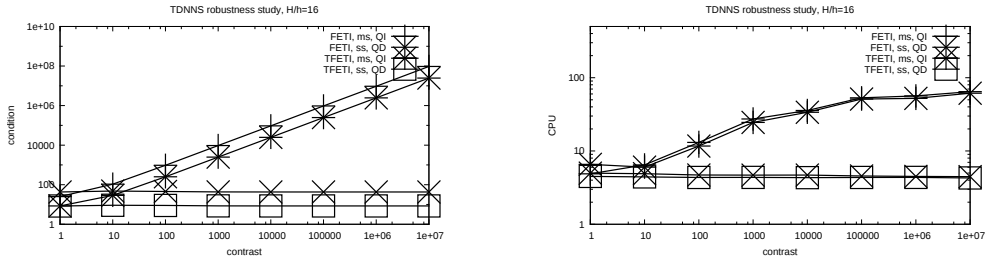

FIG. 6.2. *Robustness study, Sect. 6.2. Plot of condition numbers (left) and CPU time (right) for varying contrast (x-axis); ms: multiplicity scaling, ss: stiffness scaling, QI:* $\underline{\mathbf{Q}} = \underline{\mathbf{I}}$*, QD:* $\underline{\mathbf{Q}} = \underline{\mathbf{Q}}_{\mathrm{diag}}$.

6.3. Almost Incompressible Case. In [38] it is shown that TDNNS is applicable also in the nearly incompressible case when adding a consistent stabilization term: bilinear and linear form from equations (3.11), (3.12) are replaced by

(6.1)

$$\mathcal{A}^s(\underline{\boldsymbol{\sigma}}, (\mathbf{u}, \overline{u}_n); \underline{\boldsymbol{\tau}}, (\mathbf{v}, \overline{v}_n)) := \mathcal{A}(\underline{\boldsymbol{\sigma}}, (\mathbf{u}, \overline{u}_n); \underline{\boldsymbol{\tau}}, (\mathbf{v}, \overline{v}_n)) + \sum_{T \in \mathcal{T}_h} h^2 \int_T \mathbf{div}\underline{\boldsymbol{\sigma}} \cdot \mathbf{div}\underline{\boldsymbol{\tau}}\, ds,$$

(6.2)

$$\mathcal{F}^s(\mathbf{v}, \overline{v}_n) := \mathcal{F}(\mathbf{v}, \overline{v}_n) - \sum_{T \in \mathcal{T}_h} h^2 \int_T \mathbf{f}_V \cdot \mathbf{div}\underline{\boldsymbol{\tau}}\, ds.$$

In the current example we use the geometric setup and subdomain decomposition from Figure 6.1. We use a fixed discretization with $H/h = 8$. In the light shaded region, we set $E_1 = 10$ N/mm and $\nu_1 = 0.3$. In the dark shared region, we set $E_2 = 2 \cdot 10^5$ N/mm and vary Poisson's ratio ν_2 in the range [0.3, 0.49999].

The results for FETI and TFETI are summarized in Table 6.3. We see that neither the stiffness scaling nor the choice $\underline{\mathbf{Q}} = \underline{\mathbf{Q}}_{\mathrm{diag}}$ (as proposed in Sect. 4.5) are suitable for the almost incompressible case. However, if we use the combination of coefficient scaling and $\underline{\mathbf{Q}} = \underline{\mathbf{M}}^{-1}$, then the method is not only robust with respect to the contrast in Young's modulus, but additionally rather stable with respect to the contrast in Poisson's ratio.

REFERENCES

[1] S. Adams and B. Cockburn. A mixed finite element method for elasticity in three dimensions. *Journal of Scientific Computing*, 25(3):515–521, 2005.

[2] D. N. Arnold, G. Awanou, and R. Winther. Finite elements for symmetric tensors in three dimensions. *Math. Comp.*, 77(263):1229–1251, 2008.

[3] D. N. Arnold and R. Winther. Mixed finite elements for elaticity. *Numer. Math*, 92:401–419, 2002.

[4] D. Braess. *Finite Elements. Theory, Fast Solvers, and Applications in Solid Mechanics*. Cambridge University Press, 2007.

[5] J. H. Bramble, J. E. Pasciak, and A. H. Schatz. The construction of preconditioners for elliptic problems by substructuring, I. *Math. Comp.*, 47(175):103–134, 1986.

[6] S. C. Brenner. Poincaré-Friedrichs inequalities for piecewise H^1 functions. *SIAM J. Numer. Anal.*, 41(1):306–324, 2003.

[7] S. C. Brenner. Korn's inequalities for piecewise H^1 vector fields. *Math. Comp.*, 73(247):1067–1087, 2004.

[8] F. Brezzi and M. Fortin. *Mixed and Hybrid Finite Element Methods*. Springer, New-York, 1991.

TABLE 6.3
Results for Sect. 6.3, fixed discretization $H/h = 8$.

		FETI			TFETI		
parameters	ν_2	cond	iter	CPU	cond	iter	CPU
	0.3	22.99	26	4.36	7.70	22	4.23
	0.4	22.96	27	4.43	7.70	23	4.28
coefficient	0.45	25.32	29	4.56	7.70	24	4.34
scaling	0.49	27.47	37	5.09	14.30	31	4.82
$\underline{\mathbf{Q}} = \underline{\mathbf{Q}}_{\text{diag}}$	0.499	125.83	61	6.69	124.47	56	6.50
	0.4999	1241.1	91	8.68	1229.37	89	8.72
	0.49999	12393.6	128	11.16	12275.8	113	10.32
	0.3	25.63	25	4.28	7.44	22	4.22
	0.4	24.62	28	4.49	7.43	23	4.29
stiffness	0.45	23.76	28	4.50	7.43	24	4.36
scaling	0.49	20.97	37	5.10	15.46	33	4.96
$\underline{\mathbf{Q}} = \underline{\mathbf{Q}}_{\text{diag}}$	0.499	125.72	58	6.48	126.71	59	6.72
	0.4999	1203.67	172	14.12	1202.93	157	13.27
	0.49999	32659.6	394	28.86	9427.33	332	25.19
	0.3	5.84	18	5.81	6.06	21	6.44
	0.4	5.85	18	5.79	6.06	21	6.42
coefficient	0.45	5.85	19	5.95	6.06	21	6.41
scaling	0.49	5.85	19	5.95	6.06	23	6.69
$\underline{\mathbf{Q}} = \underline{\mathbf{M}}^{-1}$	0.499	5.94	20	6.21	14.31	24	6.84
	0.4999	6.59	20	6.07	15.76	25	6.98
	0.49999	9.10	21	6.25	15.92	25	6.97
	0.3	5.84	18	5.93	6.06	21	6.44
	0.4	5.84	18	5.90	6.06	21	6.40
stiffness	0.45	5.88	19	5.93	6.06	21	6.42
scaling	0.49	7.30	21	6.20	8.14	23	6.71
$\underline{\mathbf{Q}} = \underline{\mathbf{M}}^{-1}$	0.499	15.93	26	6.89	14.41	26	7.12
	0.4999	357.02	89	15.63	53.81	63	12.18
	0.49999	20809.7	398	58.36	3176.76	234	36.02

[9] T. Cluzeau, V. Dolean, F. Nataf, and A. Quadrat. Symbolic methods for developing new domain decomposition algorithms. Research report RR-7953, INRIA, France, 2012. `http://hal.inria.fr/hal-00694468`.

[10] T. Cluzeau, V. Dolean, F. Nataf, and A. Quadrat. Symbolic techniques for domain decomposition methods. In R. Bank, M. Holst, O. Widlund, and J. Xu, editors, *Domain Decomposition Methods in Science and Engineering XX*, volume 91 of *LNCSE*, pages 27–38. Springer, Berlin Heidelberg, 2013. `http://www.ddm.org/DD20/proceedings/articles/Cluzeau.pdf`.

[11] C. R. Dohrmann. A preconditioner for substructuring based on constrained energy minimization. *SIAM J. Sci. Comput.*, 25(1):246–258, 2003.

[12] C. R. Dohrmann and O. B. Widlund. Hybrid domain decomposition algorithms for compressible and almost incompressible elasticity. *Int. J. Numer. Meth. Engrg.*, 82:157–183, 2010.

[13] Z. Dostál, D. Horák, and R. Kučera. Total FETI – An easier implementable variant of the FETI method for numerical solution of elliptic PDE. *Commun. Numer. Methods Eng.*, 22(12):1155–1162, 2006.

[14] C. Farhat and M. Géradin. On the general solution by a direct method of a large scale singular system of linear equations: application to the analysis of floating structures. *Internat. J. Numer. Methods Engrg.*, 41(4):675–696, 1998.

[15] C. Farhat, M. Lesoinne, P. Le Tallec, K. Pierson, and D. Rixen. FETI-DP: A dual-primal unified FETI method I: A faster alternative to the two-level FETI method. *Internat. J. Numer. Methods Engrg.*, 50(7):1523–1544, 2001.

[16] C. Farhat and F. Roux. A method of finite element tearing and interconnecting and its parallel solution algorithm. *Internat. J. Numer. Methods Engrg.*, 32(6):1205–1227, 1991.

[17] C. Farhat and F. Roux. Implicit parallel processing in structural mechanics. In J. T. Oden, editor, *Computational Mechanics Advances 2*, volume 2, pages 1–124. North-Holland, Amsterdam, 1994.

[18] S. Gippert, A. Klawonn, and O. Rheinbach. Analysis of FETI-DP and BDDC for linear elas-

ticity in 3D with almost incompressible components and varying coefficients inside subdomains. *SIAM J. Numer. Anal.*, 50(5):2208–2236, 2012.
[19] W. Hackbusch. *Multi-Grid Methods and Applications*. Springer, Berlin, second edition, 2003.
[20] P. Hauret and F. Hecht. A discrete differential sequence for elasticity based upon continuous displacements. *SIAM J. Sci. Comput.*, 35(1):291–341, 2012.
[21] T. J. R. Hughes. *The Finite Element Method – Linear Static and Dynamic Finite Element Analysis*. Dover Publications, 2000.
[22] P. W. Jones. Quasiconformal mappings and extendability of functions in Sobolev spaces. *Acta Math.*, 147:71–88, 1981.
[23] A. Klawonn, O. Rheinbach, and O. B. Widlund. An analysis of a FETI-DP algorithm on irregular subdomains in the plane. *SIAM J. Numer. Anal.*, 46(5):2484–2504, 2008.
[24] A. Klawonn, O. Rheinbach, and B. Wohlmuth. Dual-primal iterative substructuring for almost incompressible elasticity. In D. Keyes and O. Widlund, editors, *Domain Decomposition Methods in Sciences and Engineering XVI*, volume 55 of *LNCSE*, pages 399–406. Springer, Heidelberg, 2007.
[25] A. Klawonn and O. B. Widlund. A domain decomposition method with Lagrange multipliers and inexact solvers for linear elasticity. *SIAM J. Sci. Comput.*, 22(4):1199–1219, 2000.
[26] A. Klawonn and O. B. Widlund. FETI and Neumann-Neumann iterative substructuring methods: connections and new results. *Comm. Pure Appl. Math.*, 54(1):57–90, 2001.
[27] A. Klawonn and O. B. Widlund. Dual-primal FETI methods for linear elasticity. *Comm. Pure Appl. Math.*, 59(11):1523–1572, 2006.
[28] R. Kučera, T. Kozubek, A. Markopoulos, and J. Machalová. On the Moore-Penrose inverse in solving saddle-point systems with singular diagonal blocks. *Numer. Linear Algebra Appl.*, 19(4):677–699, 2012.
[29] J. Mandel and M. Brezina. Balancing domain decomposition for problems with large jumps in coefficients. *Math. Comp.*, 65:1387–1401, 1996.
[30] J. Mandel and R. Tezaur. Convergence of a substructuring method with Lagrange multipliers. *Numer. Math.*, 73(4):473–487, 1996.
[31] J. C. Nédélec. A new family of mixed finite elements in $\mathbb{R}^3$. *Numerische Mathematik*, 50:57–81, 1986.
[32] G. Of and O. Steinbach. The all-floating boundary element tearing and interconnecting method. *J. Num. Math.*, 17(4):277–298, 2009.
[33] A. Pechstein and J. Schöberl. Tangential-displacement and normal-normal-stress continuous mixed finite elements for elasticity. *Math. Models Methods Appl. Sci.*, 21(8):1761–1782, 2011.
[34] A. Pechstein and J. Schöberl. Anisotropic mixed finite elements for elasticity. *International Journal for Numerical Methods in Engineering*, 90(2):196–217, 2012.
[35] C. Pechstein. *Finite and Boundary Element Tearing and Interconnecting Solvers for Multiscale Problems*, volume 90 of *LNCSE*. Springer, Heidelberg, 2013.
[36] C. Pechstein and R. Scheichl. Analysis of FETI methods for multiscale PDEs. *Numer. Math.*, 111(2):293–333, 2008.
[37] O. Schenk and K. Gärtner. On fast factorization pivoting methods for sparse symmetric indefinite systems. *Electronic Transactions on Numerical Analysis*, 23:158–179, 2006.
[38] A. Sinwel. *A New Family of Mixed Finite Elements for Elasticity*. PhD thesis, Johannes Kepler University Linz, 2009. Published by Südwestdeutscher Verlag für Hochschulschriften, June 2009, `http://www.numa.uni-linz.ac.at/Teaching/PhD/Finished/sinwel-diss.pdf`.
[39] A. Toselli and O. B. Widlund. *Domain Decomposition Methods – Algorithms and Theory*, volume 34 of *Springer Series in Computational Mathematics*. Springer, Berlin, 2005.
[40] P. S. Vassilevski. *Multilevel Block Factorization Preconditioners*. Springer, New York, 2008.